LIÈGE université Library

https://lib.uliege.be

https://matheo.uliege.be

# A 2024 Subsurface Warm and Saline Anomaly in the Ionian Sea: Origin, Gyre Dynamics and its Possible Link to the 2022 Marine Heatwave

**Auteur :** Genet, Zoé
**Promoteur(s) :** 32341; Alvera Azcarate, Aida
**Faculté :** Faculté des Sciences
**Diplôme :** Master en océanographie, à finalité approfondie
**Année académique :** 2025-2026
**URI/URL :** http://hdl.handle.net/2268.2/26876

*Avertissement à l'attention des usagers :*

*Tous les documents placés en accès ouvert sur le site le site MatheO sont protégés par le droit d'auteur. Conformément aux principes énoncés par la "Budapest Open Access Initiative"(BOAI, 2002), l'utilisateur du site peut lire, télécharger, copier, transmettre, imprimer, chercher ou faire un lien vers le texte intégral de ces documents, les disséquer pour les indexer, s'en servir de données pour un logiciel, ou s'en servir à toute autre fin légale (ou prévue par la réglementation relative au droit d'auteur). Toute utilisation du document à des fins commerciales est strictement interdite.*

*Par ailleurs, l'utilisateur s'engage à respecter les droits moraux de l'auteur, principalement le droit à l'intégrité de l'oeuvre et le droit de paternité et ce dans toute utilisation que l'utilisateur entreprend. Ainsi, à titre d'exemple, lorsqu'il reproduira un document par extrait ou dans son intégralité, l'utilisateur citera de manière complète les sources telles que mentionnées ci-dessus. Toute utilisation non explicitement autorisée ci-avant (telle que par exemple, la modification du document ou son résumé) nécessite l'autorisation préalable et expresse des auteurs ou de leurs ayants droit.*

University of Liège

Master's Degree Thesis

# A 2024 Subsurface Warm and Saline Anomaly in the Ionian Sea: Origin, Gyre Dynamics and its Possible Link to the 2022 Marine Heatwave


Author: Zoé Genet

Supervisor at OGS: Annunziata Pirro

Supervisor at ULiège: Aida Alvera-Azcárate

Review panel: Sylvie Gobert, Michel Marengo, Charles Troupin


*A thesis submitted in fulfillment of the requirements for the*

Master's Degree in Oceanography

*in the*

Faculty of Sciences

August 2026

According to the rules imposed by the jury of the Master in Oceanography, this document must not exceed 50 pages in Times 12 or an equivalent font.

# Acknowledgments

I would first like to thank my supervisor at OGS, Annunziata Pirro, for her invaluable support throughout my research, for always taking the time to explain concepts I didn't understand and for making me feel so welcome in Trieste. I would also like to thank my supervisor at ULiège, Aida Alvera-Azcárate, for her valuable advice, feed-back and kind supervision. My thanks also go to Milena Menna, who took the time to discuss the Ionian Sea with me, read my thesis and share precious material. I would also like to thank Riccardo Martellucci, for his advice and the shared material, and Abel Dechenne for explaining his research on the Ionian Sea to me. I am also very grateful to the PhD students at OGS for welcoming me into their group and making my time in Trieste so enjoyable. Finally, I would like to thank my sister, my mom, my dad and my lovely friends for their constant support.

# Table of contents

Acknowledgments....2
Table of contents....3
Abstract....5
French abstract....6
List of acronyms....7
1. Introduction....7
1.1 The Mediterranean Sea: overall current circulation....7
1.2 The Ionian Sea....10
1.2.1 The Adriatic-Ionian Bimodal Oscillating System....10
1.2.2 The circulation in the Ionian Sea....11
1.2.3 The Pelops gyre and connection with the Levantine Intermediate Water....13
1.3 Climate change in the Mediterranean Sea and marine heatwaves....14
1.3.1 The Mediterranean Sea as a hotspot for climate change....14
1.3.2 Marine heatwaves in the Mediterranean Sea....15
1.3.3 The 2022 Mediterranean marine heatwave....17
1.3.4 Temperature anomalies propagation in deeper sea layers....17
1.4 Aim of the work....20
2. Material and method....22
2.1 Study area....22
2.2 Data used....22
2.2.1 Deep currents....23
2.2.2 Absolute dynamic topography and surface currents....23
2.2.3 Heat fluxes and winds....24
2.2.4 Climatology....24
2.2.5 Temperature and salinity from Argo floats....25
2.3 Method of analysis....26
2.3.1 Hovmöller diagrams of temperature and salinity....26
2.3.2 The air-sea heat flux budget....26
2.3.3 Water transport through the borders of the box....26
2.3.4 Deep currents and temperature and salinity from Argo data....27
3. Results....28
3.1 Warm and salinity anomalies in the Ionian Sea....28

3.2 Air-sea interactions....28
3.2.1 Heat fluxes....28
3.2.2 Winds....29
3.3 Sea surface processes: surface currents and absolute dynamic topography....31
3.4 Deep currents....33
3.5 Transport....35
3.6 Temperature and salinity derived from Argo floats data....37
4. Discussion....41
4.1 Atmospheric processes: heat fluxes and wind....41
4.2 Characterizing the anomaly: in-situ evidence and data limitations....42
4.3 Structure and dynamics of the gyre....43
4.3.1 At the surface....43
4.3.2 In deeper layers....44
4.4 Onset and persistence of the anomaly....44
4.4.1 Vertical structure and candidate dynamical mechanisms: the heton framework and vorticity conservation....45
4.5 Characteristics of the water masses....47
4.6 Water current into the central Ionian....48
4.7 General warming and salinification of the Ionian Sea....48
5. Conclusion and perspectives....50
References....52
Contributions....60
Appendix....61

# Abstract

The origin of an anomalously warm and saline water mass (approximately +1°C and +0.4 psu relative to the climatology) observed by Argo floats at depths of 300-1000 m in the central Ionian Sea was investigated. The anomaly seems to have emerged in April 2024 and persisted until at least December 2024. The Mediterranean Sea is considered a climate hotspot because of its particular vulnerability to climate change. In particular, the 2022-2024 period was characterized by persistent Marine heatwave (MHW) conditions, which may have contributed to the development of the 2024 subsurface anomaly. To investigate its origin and evolution, several atmospheric and oceanic variables were studied including wind and current fields, heat fluxes, absolute dynamic topography (ADT) and water transport. The results suggest that the warm and salty water may have come from the Levantine basin, may have been downwelled in the Pelops Gyre (PG) especially during the 2022 MHW, and subsequently advected toward the central Ionian Sea. Furthermore, current fields and ADT maps revealed a persistent anticyclonic circulation in the central Ionian Sea extending to approximately 700 m depth, below which the circulation reversed and became cyclonic. This counter-rotating vertical structure may have contributed to the confinement and persistence of the anomalous water mass by limiting its dispersion. Overall, these results provide insights into the potential for MHW-related anomalies to persist at greater depths and over longer timescales than those observed at the surface, while highlighting the unusual vertical circulation structure associated with the anomaly and the particular dynamical setting of the Ionian Sea, a key region for the exchange and redistribution of water masses within the Mediterranean.

# French abstract

Dans ce travail, l'origine d'une masse d'eau anormalement chaude et salée (environ +1 °C et +0,4 psu par rapport à la climatologie) observée par les balises Argo à des profondeurs comprises entre 300 et 1000 m dans le centre de la mer Ionienne a été étudiée. Cette anomalie semble être apparue en avril 2024 et avoir persisté au moins jusqu'en décembre 2024. La Méditerranée est considérée comme un hotspot climatique en raison de sa vulnérabilité particulière au changement climatique. La période 2022-2024 a notamment été marquée par des conditions persistantes de vague de chaleur marine (MHW), qui ont pu contribuer au développement de l'anomalie subsurface de 2024. Afin d'étudier son origine et son évolution, plusieurs variables atmosphériques et océaniques ont été analysées, notamment les champs de vent et de courants, les flux thermiques, la topographie dynamique absolue (ADT) et le transport d'eau. Les résultats suggèrent que l'eau chaude et salée pourrait provenir du bassin levantin, avoir été entraînée vers les profondeurs par des processus de downwelling dans le gyre du Péloponnèse (PG), en particulier pendant la MHW de 2022, puis transportée vers le centre de la mer Ionienne. De plus, les champs de courants et les cartes d'ADT ont révélé une circulation anticyclonique persistante dans la partie centrale de la mer Ionienne s'étendant jusqu'à environ 700 m de profondeur, en dessous de laquelle la circulation s'inverse pour devenir cyclonique. Cette structure verticale caractérisée par deux circulations de sens opposés pourrait avoir contribué au confinement et à la persistance de la masse d'eau anormale en limitant sa dispersion. Dans l'ensemble, ces résultats apportent un éclairage sur la possibilité que des anomalies liées aux MHWs persistent à des profondeurs plus importantes et pendant de longues périodes, tout en soulignant la structure inhabituelle de la circulation verticale associée à cette anomalie ainsi que le contexte dynamique particulier de la mer Ionienne, une région clé pour l'échange et la redistribution des masses d'eau en Méditerranée.

# List of acronyms

| | |
|---|---|
| Atlantic Water | AW |
| Sicily Channel | SC |
| Levantine Intermediate Water | LIW |
| Levantine Surface Water | LSW |
| Atlantic Ionian Stream | AIS |
| Mid Ionian Jet | MIJ |
| Marine Heatwave | MHW |
| Absolute Dynamical Topography | ADT |

# 1. Introduction

## 1.1 The Mediterranean Sea: overall current circulation

The Mediterranean Sea is a semi-enclosed basin, connected to the Atlantic Ocean only through the Gibraltar Strait, which is ~60 km long and 14.3 km wide at the narrowest part. In this basin, unique oceanographic processes take place, as well as a complex circulation pattern that can be compared with those of the global ocean on smaller spatial and temporal scales. The large-scale circulation of the Mediterranean Sea is driven by thermohaline processes and can be approximated by a two-layer system, schematized in Figure 1 (Pinardi et al., 2015; Millot and Taupier-Letage, 2005). On the surface, confined to the upper 50-100 meters layer, fresh Atlantic Water (hereafter AW) inflows from the Gibraltar strait and travels eastward (Pinardi et al., 2015). While progressing within the basin, the incoming AW is continuously modified by the interactions with the atmosphere or by the mixing with other water masses. It is seasonally warmed or cooled during its course to the east, and its salt content increases overall, up to 38-39 psu: two units higher than at the Gibraltar strait (Jordà et al., 2017). Since it gets denser, this modified AW tends to sink. This dense and salty

water produced in the eastern part of the basin, called the Levantine Intermediate Water (LIW), then flows westward and eventually exits the basin through the Gibraltar Strait (Astraldi et al., 1999; Pinardi et Masetti, 2000; Millot and Taupier-Letage, 2005).

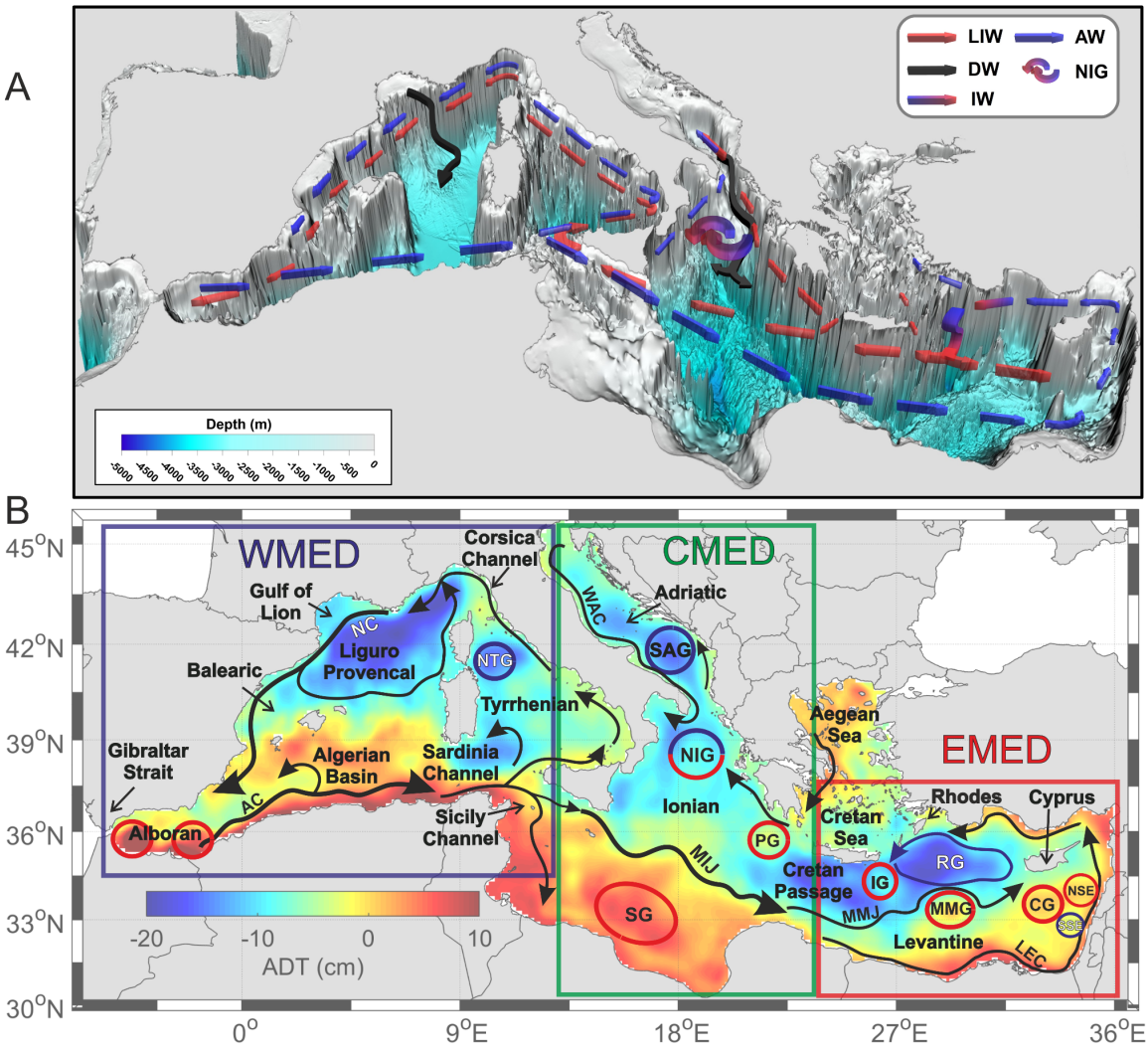


Figure 1: (A) Schematic representation of the thermohaline circulation in the Mediterranean Sea where the intermediate and deep-water formation sites are highlighted. (B) Geography of the Mediterranean Sea superimposed on the colored mean Absolute Dynamic Topography map for 1993-2019; a schematic representation of the main currents and circulation structures are depicted with black arrows and red (anticyclonic) and blue (cyclonic) circles; geographical extension of the three main sub-basins: WMED, EMED, and CMED *(which is, in our text, included in the Eastern subbasin)*. Acronyms: AW, Atlantic Water; LIW, Levantine Intermediate Water; DW, dense water; IW, Intermediate Water; NIG, Northern Ionian Gyre; AC, Algerian Current; NC, Northern Current; NTG, Northern Tyrrhenian Gyre; SG, Sidra Gyre; MIJ, Mid-Ionian-Jet; SAG, Southern Adriatic Gyre; WAC, Western Adriatic Current; PG,

Pelops Gyre; MMJ, Mid-Mediterranean Jet; LEC, Libyo-Egyptian Current; IG, Ierapetra Gyre; RG, Rhodes Gyre; MMG, Mersa-Matruh Gyre; CG, Cyprus Gyre; SSE, South Shikmona Eddy; and NSE, North Shikmona Eddy. Figure from Menna et al. (2022).

The Mediterranean Sea is divided in two subbasins (the western and the eastern) by the Sicily Channel (SC), which is located in the center of the Mediterranean Basin, between Tunisia and Sicily. The SC is characterized by a sill of about 400 meters depth, which acts like a physical barrier. Indeed, the reduced depth of its continental shelf plays a major role in constraining the large-scale circulation, as it modulates the exchange of surface and intermediate waters between the two Mediterranean subbasins (Astraldi et al., 1999). The SC links the respective large-scale cyclonic circulations of the two subbasins: using the same two-layer approximation introduced above, the eastward flow with low-density AW in the top layer is superposed to a westward flow of higher-density intermediate water, dominated by the LIW (Malanotte-Rizzoli et al., 1997; Astraldi et al., 2002; Béranger et al., 2005; Menna and Poulain, 2010; Jouini et al., 2016;) However, since the SC is relatively shallow, it does not allow the dense deep waters (~1000 meters) formed respectively in the eastern and western Mediterranean to travel to the other basin (Tsimplis et al., 2006).

The LIW, located in the eastern basin, is the warmest and saltiest intermediate water. It is produced in large quantities and is recognised almost everywhere in the Mediterranean Sea because of its characteristics. The LIW is found just below the AW, at a depth of around 300-400 meters, and hence mixes with it as soon as the AW begins to sink (Lascaratos et al., 1993; Millot and Taupier-Letage, 2005).

Numerous cyclonic and anticyclonic gyres and eddies are found in the open ocean, while the currents are strong at the border of the domain (Figure 1). Note that in this work, the term *gyre* is used for relatively large-scale and persistent rotating circulation features located in a fixed geographical area, whereas *eddy* refers to more localized and transient rotating structures. The term *eddy* may also be used as a generic term referring to rotating structures, with no consideration to their scale or persistence. Over the whole sea, most studies report current velocities below 1 m/s. The currents are largely constrained by the coastlines and the continental slopes, because of the complex bathymetry of the area.

## 1.2 The Ionian Sea

### 1.2.1 The Adriatic-Ionian Bimodal Oscillating System

Overall, thermohaline processes and the complex circulation patterns in the Mediterranean Sea are known to be subject to changes and cannot be studied from a static perspective. A perfect example of this dynamic view is the reversal of the North Ionian Gyre (NIG), which seems to be mainly caused by the Adriatic-Ionian Bimodal Oscillating System (BiOS; Gačić et al., 2010; Meli, 2024).

The Ionian Sea is located in the eastern basin of the Mediterranean Sea and is bounded by Sicily to the west, the Adriatic to the north, the west coast of Greece, including the Peloponnese, to the east, the Levantine basin to the south and the Aegean basin to the south-east. It is the deepest sub-basin of the Mediterranean Sea (reaching depths of 4500 m), covers an area of more than 200 000 $km^2$ and consists of several trenches and plateaus. Due to its location in the center of the Mediterranean, the Ionian Sea serves as a crossroads for water masses coming from the east and the west Mediterranean Sea (Gačić et al., 2010; Menna et al., 2019; Civitarese et al., 2023; Eusebi Borzelli et al., 2025; Terzić and Vilibić, 2026). Furthermore, the surface current circulation of the north Ionian Sea seems to have a significant impact on the thermohaline properties and water mass redistribution in the Mediterranean, particularly the NIG reversal (Eusebi Borzelli et al., 2009; Civitarese et al., 2010; Gačić et al., 2010). In recent decades (at least since the late 1980s), the NIG shifts between a cyclonic and an anticyclonic mode (Gačić et al., 2010; Menna et al., 2019; Meli, 2024). This phenomenon appears to have a quasi-decadal scale, although it has recently seen shorter variations and is becoming milder (Liu et al., 2022; Meli, 2024; Napolitano et al., 2025; Menna et al., 2026). NIG patterns influence the biogeochemistry of the Mediterranean Sea (Civitarese et al., 2023), particularly in the Ionian Sea through large-scale shifts of the nutricline (Civitarese et al., 2010; Lavigne et al., 2018), with potential impacts on the Mediterranean marine ecosystems (Lavigne et al. 2018).

The NIG reversals are primarily driven by internal processes, the most important of which is the BiOS, a feedback mechanism linking the circulation of the Northern Ionian Sea with the exchange of water masses between the Ionian and Adriatic Seas (Civitarese et al., 2010; Gačić et al., 2010). Through alternating cyclonic

and anticyclonic circulation regimes, the BiOS regulates the advection of relatively fresh AW and saltier Levantine waters (the LIW and the Levantine Surface Water, or LSW), toward the Adriatic Sea, thereby influencing dense water formation and the subsequent evolution of the Ionian circulation (Gačić et al., 2010; Menna et al., 2019; Menna et al., 2022; Civitarese et al., 2023). By modulating the advection of distinct water masses, the BiOS affects not only plankton phenology but also community composition and higher trophic levels, including zooplankton and fish populations (Batistić et al., 2014; Lavigne et al., 2018; Patti et al., 2025).

### 1.2.2 The circulation in the Ionian Sea

The AW that crosses the SC and enters the eastern basin can be separated into two jets: the Atlantic Ionian Stream (AIS), which is directed by the Sicily continental slope, and the Atlantic Tunisian Current, that follows the Tunisian coastline (Jouini et al., 2016; Jebri et al., 2017; Martínez et al., 2024).

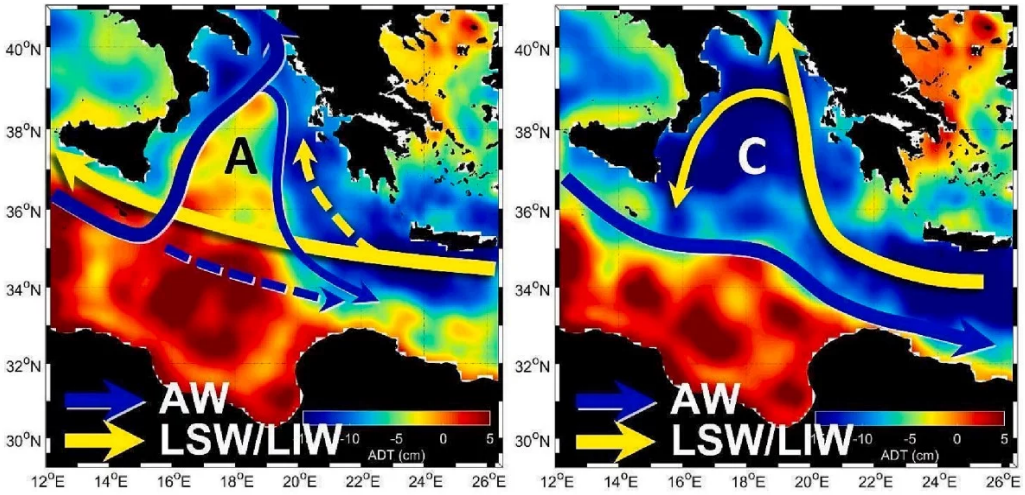


Figure 2: Schematic representation of the two circulation modes in the Ionian Sea. A: anticyclonic circulation (left); C: cyclonic circulation (right). The effects of circulation reversal are the variation of AW and LIW paths. Annual mean ADT distributions in 1995 (left) and 1999 (right) are shown in the background. Figure from Menna et al. (2019).

In the Ionian Sea, as mentioned, the surface circulation varies between two modes: cyclonic or anticyclonic. During cyclonic phases, most of the AIS coming from the SC follows a direct short route to the Levantine basin, crossing the eastern basin in its central part (in the southern Ionian Sea), and arrives well organized and most intense (10-20cm/s): this jet is called the Mid Ionian Jet (MIJ) and is surrounded by

many vortices (Gačić et al., 2010; Poulain et al., 2012; Mkhinini et al., 2014; Pinardi et al., 2015; Menna et al., 2019; Liu et al., 2022; Civitarese et al., 2023). The cyclonic NIG favors the spreading of the high saline LIW into the North Ionian basin, which then enters the southern Adriatic Sea (Figure 2; Civitarese et al., 2023; Menna et al., 2026). This high salinity water favors the formation of dense water in the deep Adriatic which, subsequently, exits the basin flowing in the Ionian Sea abyssal layers following the bathymetric contour along the Italian coastline due to the strong constraint of potential vorticity conservation. The Ionian isopycnal surfaces thus rise inducing the squeezing of the upper-layer column which decreases the vorticity and leads to anticyclonic circulation conditions (Malanotte-Rizzoli et al., 1997; Gačić et al., 2010; Liu et al., 2022; Civitarese et al., 2023; Martellucci et al., 2025).

During the anticyclonic phase of the NIG, a branch of the AIS is deflected north-eastward toward the North Ionian and Adriatic Sea with a consequent weakening of the MIJ (Figure 2; Gačić et al., 2013; Civitarese et al., 2023). This condition leads to a reduced inflow of the AW in the Levantine basin, resulting in saltier LSW and to a density decrease in the Adriatic, which produces and exports a less dense deep water. The latter eventually spreads into the Ionian Sea, isopycnal surfaces deepen, stretch the upper-layer column and lead to a reversal of the circulation from anticyclonic to cyclonic (Gačić et al., 2010; Liu et al., 2022; Civitarese et al., 2023; Menna et al., 2026). As for the LIW, most of it moves eastward directly toward the SC without entering the Ionian Sea (Civitarese et al., 2023). These different water mass circulations affect the salt content of the Ionian Sea: it is higher during the cyclonic phase, when the spreading of LIW is enhanced, and lower during the anticyclonic phase, when AW is more prevalent (Gačić et al., 2013).

Besides the circulation described above, the Ionian Sea is characterized by a distinct vertical stratification that can be approximated by a three-layer system. The upper layer is located between the surface and approximately 150 meters depth and is mostly formed by the warm and saline LSW as well as by the fresh and cold AW, which can usually be identified as a subsurface minimum of salinity. The second layer extends from ~150 to ~500 meters in depth and is made of LIW, which is recognizable by a salinity maximum. The deepest layer, from 500 meters to the bottom, consists of deep waters coming from the Adriatic or Aegean Seas (Malanotte-Rizzoli et al., 1997; Eusebi Borzelli et al., 2024).

### 1.2.3 The Pelops gyre and connection with the Levantine Intermediate Water

Water masses of Levantine origin are strongly influenced by different anticyclones in the Eastern basin. For example, the Pelops gyre (PG) (Figure 1) plays an important role in the transport of surface and intermediate waters of Levantine origin in the adjacent basins (Malanotte-Rizzoli et al., 1997; Menna et al., 2021).

The PG is an anticyclonic eddy located in the eastern Ionian Sea, southwest of the Peloponnese, has a diameter of about 80-120 km and a maximum speed around 20 cm/s. This wind-generated feature extends from the surface to depths of 800-1000 meters (Figure 3; Malanotte-Rizzoli et al., 1997, Menna et al., 2021). The upper layer of the PG (50-80 m depth) is filled by the LSW, characterized by high salinity maximum ($S > 39.1$), the largest potential temperature and potential densities smaller than 27.5 kg $m^{-3}$. The LIW layer, characterized by densities larger than 28.75 kg $m^{-3}$ and salinities of 38.9-39.05, is generally located between 250 and 450 m. Under the LIW layer, between 800 and 1000 m, the PG water has a salinity (density) between 38.85 and 38.9 psu (29.1-29.15 kg $m^{-3}$; Menna et al., 2021). Downwelling processes, driven by the anticyclonic dynamics of the gyre and enhanced during the winter season, occur in the center of this structure, affecting the physico-chemical properties of the LIW and of the LSW (Mkhinini et al., 2014; Menna et al., 2021). However, the AW is only sporadically found in the PG (Figure 3), due to its isolation from the thermohaline circulation of AW because of the gyre's geographical location (Menna et al., 2021).

The PG transports anticyclonically the LIW around its periphery and adjusts its northward pathway toward the Adriatic Sea, alongside the eastern Greek coastline (Figure 1; Malanotte-Rizzoli et al., 1997; Kalimeris et Kassis, 2020; Menna et al., 2021). Regardless of the NIG's polarization, the current remains northward (Menna et al., 2021).

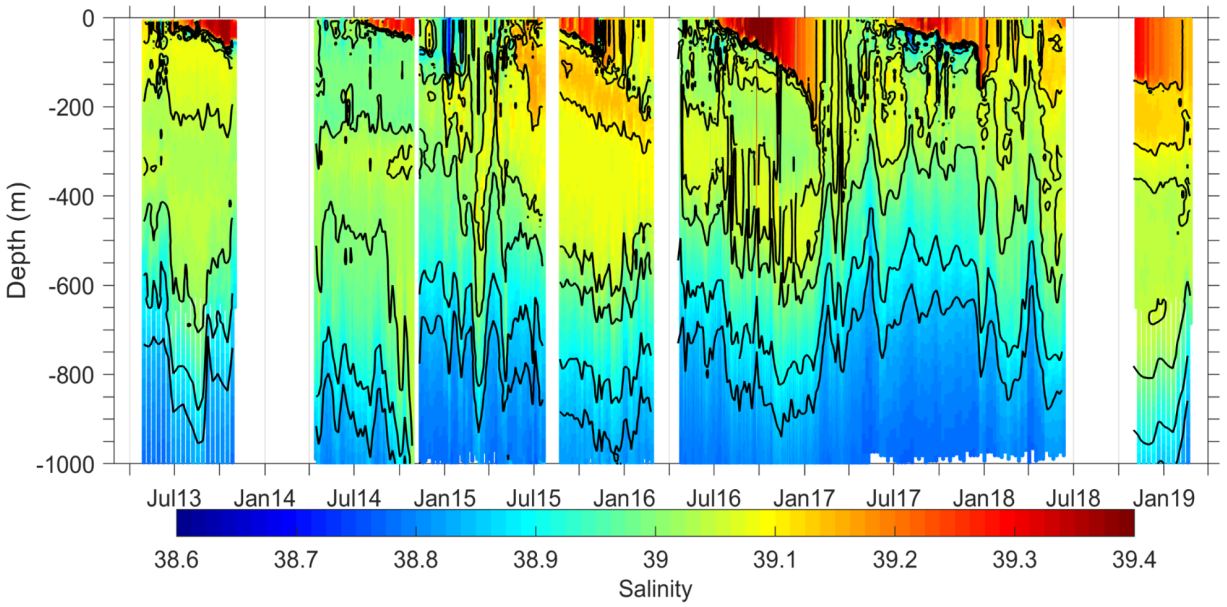


Figure 3: Contour diagrams of the salinity versus depth and time for a float entrapped in the PG. Black continuous lines are the isohalines 38.85, 39, 39.05, and 39.15. Figure from Menna et al. (2021).

## 1.3 Climate change in the Mediterranean Sea and marine heatwaves

### 1.3.1 The Mediterranean Sea as a hotspot for climate change

As explained above, the circulation of the Ionian Sea and its connection to the Adriatic through the BiOS mechanism play a central role in redistributing heat and salt across the eastern Mediterranean basin. Any shift in water mass pathways or gyre polarity has the potential to influence how heat and salt anomalies propagate, persist, or dissipate within the basin. This regional variability is best understood in light of broader global trends: in recent times, the Earth system has witnessed an increase in human emissions of greenhouse gases and as a result, has been accumulating heat, with around 90% stored in the ocean (IPCC, 2021). This is particularly relevant given that the Mediterranean Sea, despite encompassing only ~0.3% of the global ocean's

total volume, is considered as a climate hotspot because it has been changing faster than the global ocean (Juza and Tintoré, 2021). Over the last two decades, the Mediterranean Sea has been characterised by increases in sea temperature, sea salinity and sea level (Pastor et al., 2018; Skliris et al., 2018; Mohamed et al., 2019). These specific conditions are due to the sea's semi-enclosed topography and its location within the transitional zone between temperate and subtropical/tropical climates. Despite covering only ~2.5 million km$^2$, the Mediterranean Sea is home to more than 17 000 marine species, featuring the highest rate of endemism in the world (United Nations Environment Programme, 2021), and to 542 million people (in 2020; Ali et al., 2023). The Mediterranean Sea is one of the most heavily exploited seas in the world, thus its marine ecosystems are of high ecological importance and represent a major socio-economic issue for coastal communities (Darmaraki et al., 2024).

### 1.3.2 Marine heatwaves in the Mediterranean Sea

Marine heatwaves (MHWs) are defined as periods during which temperatures exceed a given threshold over a sufficiently long time and spatial extent (Hobday et al., 2016). MHWs can occur in coastal and open-ocean regions, both at the surface and in deeper waters, spanning up to thousands of kilometers and inducing abrupt changes in marine biodiversity and ecosystem processes over timescales ranging from days to years (Darmaraki et al., 2024). The rise in the surface temperature of the Mediterranean Sea in the last decades has been linked to an increase in the frequency of MHW events (Ibrahim et al., 2021; Juza et al., 2022; Dayan et al., 2023; Pastor et Khodayar, 2023). Since the 1980s, the Mediterranean Sea has experienced MHWs that are more frequent, more intense and longer lasting (Androulidakis and Krestenitis, 2022; Pastor et Khodayar, 2023). As ocean warming has increased the frequency of extreme sea surface temperature events (Lima and Wethey, 2012), MHWs are more frequent and intense in the western Mediterranean, while the duration of MHWs is longer in the eastern basin (Figure 4; Hamdeno and Alvera-Azcárate, 2023).

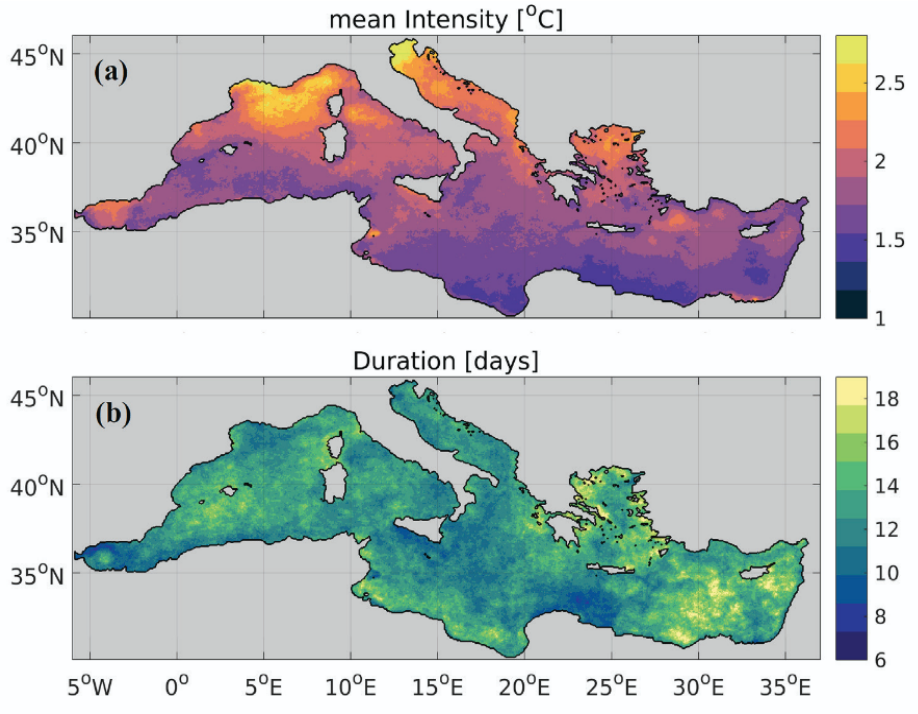


Figure 4: Mean MHW intensity (a) and duration (b) in the Mediterranean Sea averaged over 1982-2023. Figure from Darmaraki et al. (2024).

Specifically, between 1982 and 2018, the eastern basin has been warming faster (0.048 ± 0.006°C/year) compared to the western basin (0.035 ± 0.006°C/year; Pastor et al., 2020; Pisano et al., 2020). In the eastern basin, there is also a salinification trend as well as an increase in the MHW number, by 1.2 events/decade between 1982 and 2020 (Ibrahim et al., 2021). Moreover, across the Aegean, Ionian and Cretan Seas, the frequency of MHWs increased by approximately two events/decade in the 2008-2021 period (Androulidakis and Krestenitis, 2022). In the Levantine basin, LIW and LSW are warming at ~0.3°C and 1.2°C per decade and salinifying at ~0.05 and 0.03 per decade (between 1978 and 2014; Ozer et al., 2017). The deep southern Adriatic also experienced exceptional warming (0.8°C) and salinification (0.2) over the past decade, altering dense-water formation, due to increased LIW-driven salt inflow and to local freshwater and thermal forcing (Kubin et al., 2023). As for the Ionian Sea specifically, it experienced its warmest conditions of the past four decades in 2024: mean summer surface temperatures reached more than 28°C. Between 1982 and 2024, the area witnessed an increase of up to 0.59°C per decade (Terzić and Vilibić, 2026).

In the Ionian Sea, one of the notable ecological impacts of increasing sea surface temperatures is the decline of *Posidonia oceanica* seagrass (Litsi-Mizan et al., 2023). More broadly, the long-term increase in sea temperature and MHWs frequency have induced profound changes in marine ecosystems and in the services they provide to human societies (Smith et al., 2021). The intensification of surface MHW throughout the twenty-first century is therefore a cause for serious concern, especially since scientists working on future climate scenarios agree that the duration and the spatial extension of MHWs in the Mediterranean Sea are very likely to increase (Darmaraki et al., 2019).

### 1.3.3 The 2022 Mediterranean marine heatwave

In the Mediterranean Sea, summer MHWs generally result from a combination of enhanced solar radiation, light but persistent winds and limited heat loss at the surface (Darmaraki et al., 2024). The year 2022 provides an exceptional example of these processes, as the Mediterranean Sea experienced unprecedented temperatures during an exceptionally long MHW event that lasted until 2023-2024 (Figure 5; Marullo et al., 2023) The episode started in the north-western Mediterranean basin around mid-May 2022, following the suppression of northerly winds in the area, associated with anticyclonic anomalies over western-central Europe (Marullo et al., 2023). The increased shortwave radiation, light cloud cover and reduced wind speeds lessened the contribution of turbulent heat fluxes to ocean heat dissipation. The event subsequently propagated southward, reaching its highest intensity and spatial extent by July, co-occurring with a significant atmospheric heatwave over Europe (Marullo et al., 2023); southward advection of hot and humid air masses likely exacerbated the MHW (Guinaldo et al., 2023). Although the event was most intense in the western Mediterranean (Trigo et al., 2025), major impacts were also observed in the eastern basin (Marullo et al., 2023; Pirro et al., 2024).

### 1.3.4 Temperature anomalies propagation in deeper sea layers

As discussed above, MHWs are not exclusively limited to the uppermost water layers but can also extend deeper (Darmaraki et al., 2019; Juza et al., 2022; Pirro et al., 2024). Although MHW intensity generally decreases with depth, studies have shown that warm anomalies can penetrate into the deeper layers without being dissipated, through dynamical processes like downwelling or deep convection (Bakun

and Agostini, 2001; Pinardi et al., 2015; Pirro et al., 2024). While MHW frequency is higher at the surface, their duration is longer in the subsurface, sometimes persisting for several months (Darmaraki et al., 2019; Dayan et al., 2023). Dayan et al. (2023) showed that in the western Mediterranean Sea, MHW maximum intensity is most often found at the surface, while in the Levantine basin, the extremes temperature values are reached in the subsurface layers. Deep MHWs can potentially induce multiple physical consequences, like amplifying circulation changes or impacting the deep convection in the sea (Margirier et al., 2020; Josey and Schroeder, 2023) and biological consequences, like threatening biodiversity or food provision (Schaeffer and Roughan, 2017; Holbrook et al., 2020; Garrabou et al., 2022).

Juza et al. (2022) have demonstrated that MHWs occurring between 2012 and 2020 displayed an eastward subsurface development: in the western basin, MHWs extended to depths of 50-150 m but reached up to 400-700 meters in the eastern Mediterranean. The 2022 MHW has affected the entire water column in the Mediterranean Sea: the heat extended from the uppermost layers to at least 1500 meters depth (Pirro et al., 2024). The propagation of the warming to deeper layers was first caused by wind-induced vertical mixing, which also reduced the surface temperature anomaly (Marullo et al., 2023). Later, strong stratification inhibited further downward propagation and favored the persistence of warm anomalies for several months, as the upward transfer of subsurface heat and its subsequent dissipation to the atmosphere were limited (Marullo et al., 2023; Pirro et al., 2024). Significant temperature anomalies were still observed in spring 2023, especially in the southern Mediterranean (Marullo et al., 2023; Simon et al., 2023) and persisted until 2024 (Figure 5). The anticyclonic atmospheric conditions established during summer 2022 persisted throughout the following winter (Marullo et al., 2023). Heat penetration and storage within the intermediate and deep layers depend strongly on regional circulation. In areas characterized by downwelling or deep convection, heat can be rapidly redistributed throughout the water column and stored for extended periods (Pirro et al., 2024). For instance, in the PG region, vertical penetration of heat in 2022 was closely related to the gyre dynamics. Indeed, positive temperature anomalies were found in spring-summer in the first 800 m of the water column, coinciding with the vertical extension of the gyre (Pirro et al., 2024). The downward propagation of the warm anomaly resulted from the downwelling associated with the PG, a process that

subsequently permitted the deep penetration of the fall cooling into the water column, causing negative temperature anomalies in the surface layer (Pirro et al., 2024). The MHW persisted in the Mediterranean throughout 2023 (Marullo et al., 2023; Simon et al., 2023) and 2024, the magnitude of the warm anomalies increasing progressively over the three years in the PG (Figure 6). In the intermediate and deep layers of some basins, warm anomalies observed after the 2022 MHW could also result from the advection of warm waters from adjacent basins (Pirro et al., 2024), although this mechanism remains poorly documented.

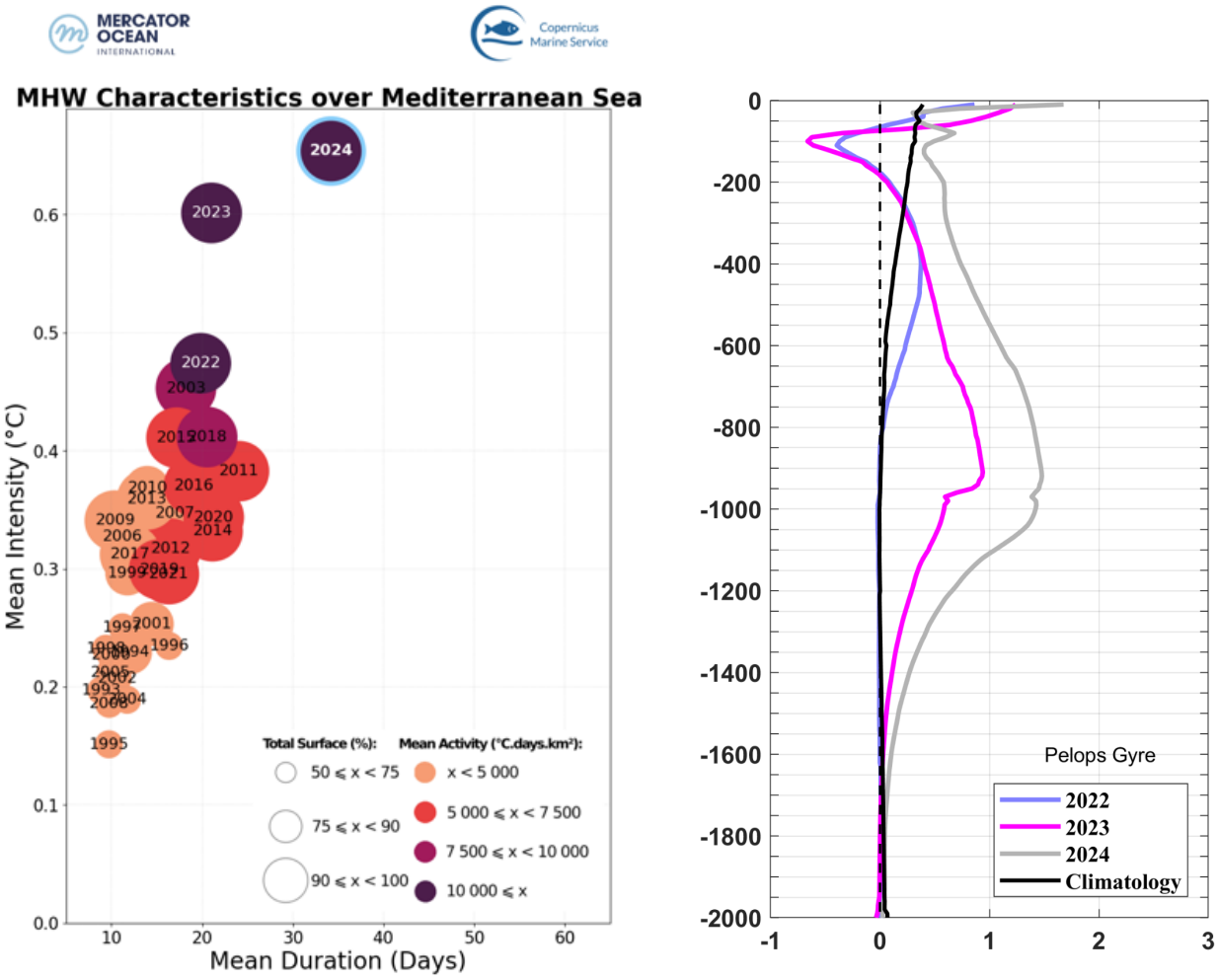


Figure 5 (left): Annual MHW Characteristics from 1993 to 2024. Duration, intensity, extent and activity averaged for each year between 1993 and 2024 for the Mediterranean Sea. 2024 is highlighted with a blue edge. Figure from Mercator Ocean International, 2025.

Figure 6 (right): Mean temperature-anomaly profiles in the PG box (34-37°N and 20-24°E, see Section 2.1), derived from Argo float observations collected in 2022, 2023, and 2024 relative to the 1985- -2018 SeaDataCloud climatology. The black profile represents the mean

temperature anomaly in the area, calculated from the historical float dataset for the period 2001-2018. Figure by Menna and Pirro, personal communication.

## 1.4 Aim of the work

While most studies on MHWs are focusing primarily on the surface layer, investigating the impacts of MHWs in deeper layers and over longer timescales is important for the reasons outlined above. When tracking subsurface warming from the 2022 MHW using Argo floats and observing its impacts through 2024, Pirro et al. (2025) highlighted anomalously high temperatures recorded in the Ionian Sea, within the 300-1000 meters depth range (Figure 7a). The warm signal, of about +1°C compared to the climatology, starts to be recorded in April 2024 and lasts until the end of the year. Not only were warm anomalies recorded, but they were also associated with unusually high salinity values, of approximately +0.4 psu relative to the climatology (Figure 7b), beginning at the same time and occurring within the same depth range.

The main objective of this work is to investigate the mechanisms responsible for the warming found in the Ionian Sea within the 300-1000m layer in 2024. With this aim, we will first examine different surface variables of the area as well as some interactions with the atmosphere: surface currents, absolute dynamic altimetry, sea surface temperatures, winds and heat fluxes. Then, we will study the currents in deeper layers, the horizontal water advection from adjacent basins and the temperature and salinity of the different water masses present in the region using in-situ data from Argo floats. Particular attention will be paid to the potential roles of horizontal advection, the role of the PG in the circulation of the central Ionian Sea as well as the possible links with waters from Levantine origins.

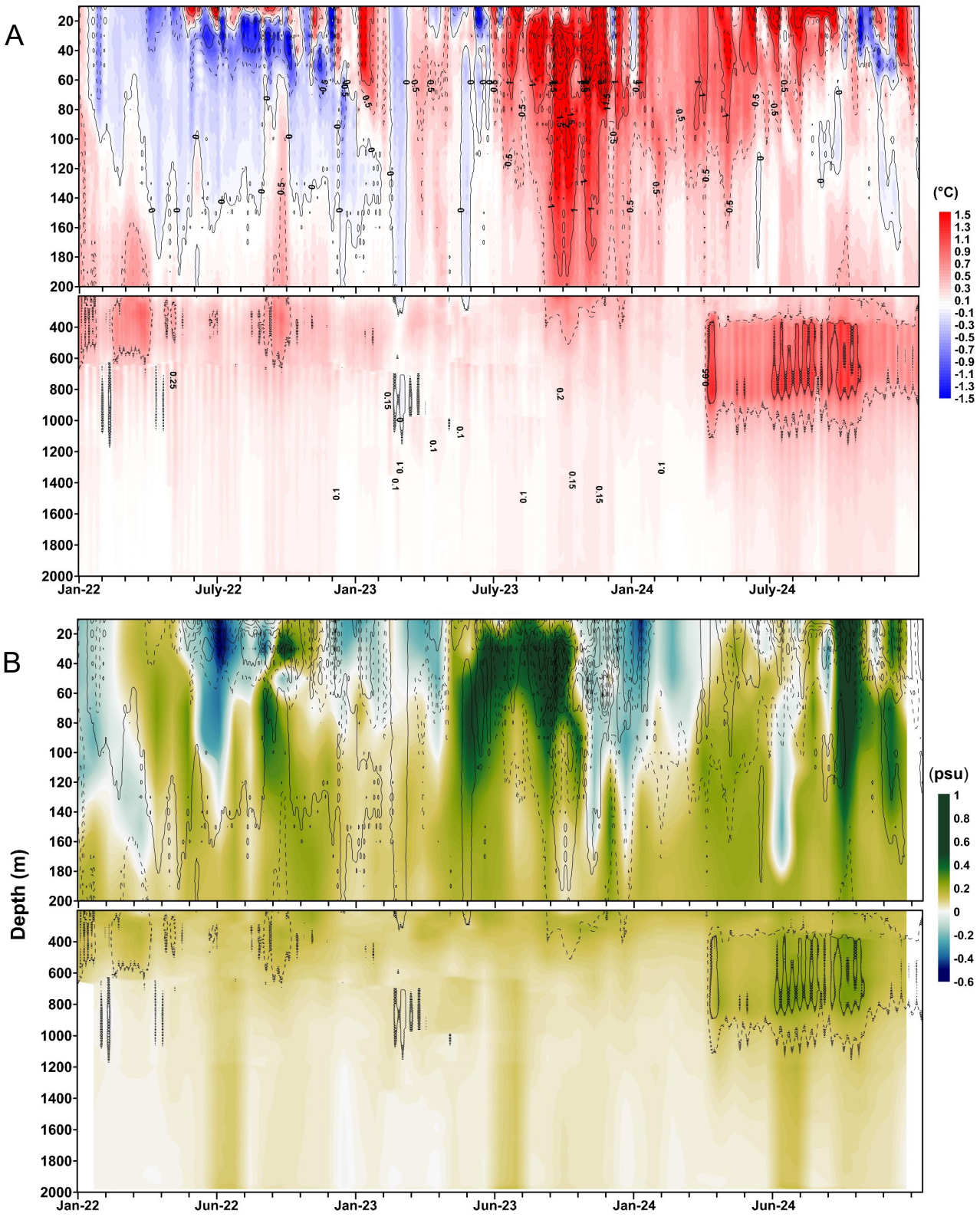


Figure 7: Temperature anomaly (A) and salinity anomaly overlaid with temperature anomaly isotherms (B) computed from Argo float data from 2022 to 2024 and average for the ION box (34-37°N and 16-20°E, see Section 2.1). The anomaly is computed with respect to the mean temperature from 1985 to 2018 from SeaDataNet data.

# 2. Material and method

## 2.1 Study area

Following the work of Pirro et al. (2025), one main study region was selected for our study, based on the spatial extent of the 2022 MHW and on availability of Argo floats: the ION box. The ION box is approximately 120 000 km$^2$ wide and is located in the middle of the Ionian Sea (34-37°N and 16-20°E). A second region was also studied in this work: the PG box. It is located in the eastern Ionian Sea (34-37°N and 20-24°E) and is also approximately 120 000 km$^2$. The two study regions are represented in Figure 8.

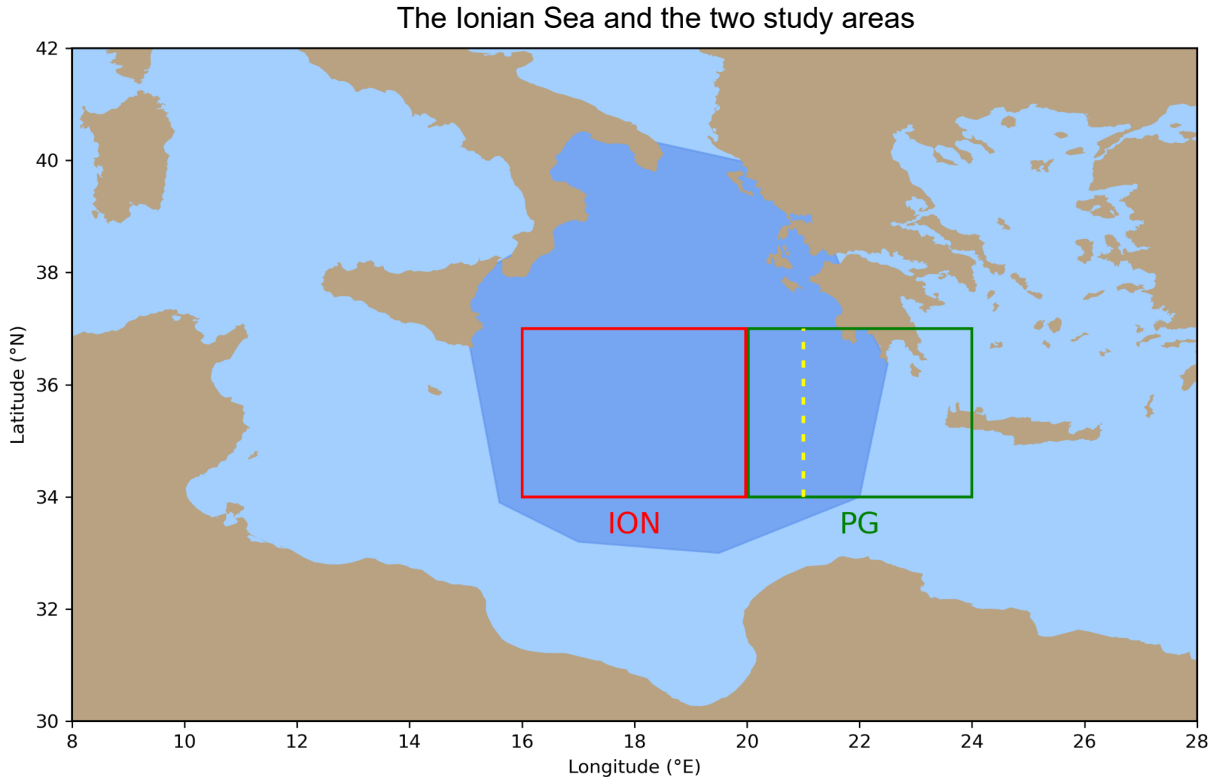


Figure 8: Study areas in the Mediterranean Sea. The ION sector is outlined in red and the PG sector in green. The Ionian Sea area is shaded in dark blue (approximate boundaries). The transect represented by the yellow dotted line will be used in Section 3.5.

## 2.2 Data used

The different datasets used for the present work are reported in Table 1 and discussed in the following subsections.

Table 1: Product data used to perform the analysis of the present work.

| Product ref. no. | Product ID, Dataset ID and type | Data access | Documentation |
|---|---|---|---|
| 1 | MEDSEA_MULTIYEAR_PHY_006_004, numerical models | EU Copernicus Marine Service Product (2026a) | Quality Information Document (QUID): Escudier et al. (2025) |
| 2 | SEALEVEL_EUR_PHY_L4_MY_008_068, numerical models | EU Copernicus Marine Service Product (2026b) | Quality Information Document (QUID): Ballarotta et al. (2025) |
| 3 | ERA5 hourly data on single levels from 1940 to present, numerical models | EU Copernicus Climate Change Service Product (2026) | Reference publication for ERA5: Hersbach et al. (2020) |
| 4 | SEADATANET_MedSea_climatology_V2, climatology | SeaDataNet Product, Simoncelli et al. (2020b) | Product Information Document (PIDoc): Simoncelli et al. (2020a) |
| 5 | INSITU_MED_PHYBGCWAV_DISCRETE_MYNRT_013_035, in-situ observations | EU Copernicus Marine Service Product (2026c) | Quality Information Document (QUID): Wehde et al. (2025) |

### 2.2.1 Deep currents

The deep currents data were obtained from the EU Copernicus Marine Service. The following variables of the Mediterranean Sea Physics Reanalysis dataset (Product n°1 in the Table 1) were used: eastward sea water velocity and northward sea water velocity. The model assimilates in-situ temperature and salinity profiles, as well as satellite altimetry observations. The model horizontal grid resolution is 0.042° (~4-5 km; Escudier et al., 2025), and the monthly temporal resolution was used.

Unlike surface-ocean models, deep-ocean models cannot be well constrained by satellite observations or High-Frequency Radar measurements. Instead, they rely largely on in situ observations, including data collected by Argo floats (see Section 2.2.5). However, Argo floats provide irregular sampling of the basin in both space and time, which can introduce biases when the data are spatially aggregated.

### 2.2.2 Absolute dynamic topography and surface currents

To map the absolute dynamic topography and the surface currents, the following dataset from the EU Copernicus Marine Service was used: the European

Seas Gridded L4 Sea Surface Heights And Derived Variables Nrt (Product n°2 in the Table 1). The variables used are the sea surface height above geoid (or ADT), the surface geostrophic eastward sea water velocity and the surface geostrophic northward sea water velocity. The variable ADT (Absolute Dynamic Topography) is measured using the concept of geoid, which is a gravity equipotential surface that would correspond with the ocean surface if the ocean was motionless, under only the gravity field. In reality, the ocean surface deviates from the geoid because it is influenced by winds, precipitation and other sources of energy: the ADT is thus the instantaneous height above the geoid. The geostrophic currents are deduced from comparisons between altimeter L4 products and drifter measurements. Since they are derived from the gridded Sea Level Anomaly field, they can be sensitive to residual noise and the noise reduction strategy applied on Sea Level Anomaly. The spatial resolution of the different variables is 0.0625°, and the data are available on a daily basis (Ballarotta et al., 2025).

### 2.2.3 Heat fluxes and winds

Wind and heat flux components were obtained from the EU Copernicus Climate Change Service (C3S) (Product n°3 in the Table 1), implemented by ECMWF, ERA5 (Hersbach et al., 2020). The variables used were the winds at 10 meters elevation (10m u-component of wind and 10m v-component of wind), the mean surface net short-wave radiation flux, the mean surface latent heat flux, the mean surface net long-wave radiation flux and the mean surface sensible heat flux. The spatial resolution of the reanalysis is 0.25°, and data were downloaded for only four hours per day: 00:00, 06:00, 12:00 and 18:00.

### 2.2.4 Climatology

The monthly temperature and salinity climatological fields for the Mediterranean Sea and for the period 1985-2018 were used. The climatological fields were derived from an integrated dataset (Product n°4 in the Table 1) combining data from the SeaDataNet infrastructure and the Coriolis Ocean Dataset for Reanalysis (CORA), version 5.2 (July 2020 update). The horizontal resolution is 0.125° (Simoncelli et al., 2020a).

### 2.2.5 Temperature and salinity from Argo floats

Table 2: information about the Argo float in our study area in 2024 (identification number of the platform, dates of *entrance into* and *exit from* the area, maximum depth, latitude and longitude at the start/end, cycle time in 2024). Data from Euro-Argo (2026).

| WMO | Start date | End date | Max depth (m) | Lat start | Lon start | Lat end | Lon end | Cycle Time in 2024 (in hours) |
|---|---|---|---|---|---|---|---|---|
| 5906993 | 01-01-24 | 06-12-24 | 1980 | 36,92 | 18,04 | 36,10 | 16,08 | 10 days |
| 5907088 | 03-01-24 | 28-03-24 | 1960 | 36,23 | 17,17 | 36,94 | 17,48 | 5 days |
| 2903797 | 04-01-24 | 29-12-24 | 1970 | 36,31 | 17,88 | 36,60 | 16,20 | J,F: 4.5 days<br>M-O: 9.5 days<br>N,D: 4.5 days |
| 6903826 | 05-01-24 | 16-06-24 | 2000 | 34,87 | 18,16 | 34,00 | 19,01 | 122 |
| 7901138 | 26-03-24 | 29-12-24 | 530 | 36,07 | 16,55 | 35,41 | 17,59 | J,F: 4<br>M-D: 29 |
| 7901139 | 26-03-24 | 17-06-24 | 540 | 35,81 | 18,87 | 34,00 | 18,69 | 4 |
| 7901140 | 27-03-24 | 30-07-24 | 420 | 35,72 | 19,59 | 34,01 | 19,74 | 4 |
| 6990629 | 29-03-24 | 31-12-24 | 2000 | 35,93 | 17,99 | 35,68 | 18,13 | M,A: 24<br>M-D: 77 |
| 6990658 | 18-08-24 | 22-12-24 | 1980 | 35,92 | 17,65 | 35,79 | 16,42 | 10 days |

Argo floats are robotic instruments that drift freely with the currents and move up and down between the surface and deeper layers of the ocean. The data (Product n°5 in the Table 1) used to make the horizontal scatter plots (Figure 17 and 18) of salinity/temperature derived by floats at certain depths come from nine Argo floats that were located in our study area during 2024 (Table 2). The resulting 2D plots are therefore sparse, but they nevertheless provide sufficient information to investigate the spatial distribution of temperature and salinity anomalies. Each float has a different cycle time, sometimes multiple during the year of 2024; they are specified in the table. These data were also used to make the two Hovmöller temperature and salinity diagrams presented in Figure 7.

## 2.3 Method of analysis

### 2.3.1 Hovmöller diagrams of temperature and salinity

The two Hovmöller diagrams, displaying the temperature and salinity at different depths in the ION box from 2022 to 2024 (Figure 7), were computed by subtracting the climatological temperature/salinity fields (climatology of 1985-2018) from the Argo observations. To obtain a regular grid, a linear interpolation every 10 m, filling the gaps of no data, was made.

### 2.3.2 The air-sea heat flux budget

The air-sea heat flux budget represents the total heat gain or loss in a given area at the sea surface (in Watt/$m^2$), so the difference between the heat coming from the sun absorbed by the sea and the thermal energy radiating from the sea surface. The chosen area is the ION box (Figure 8). To compute the total heat flux Qi, four fluxes at the surface were summed: the net short-wave radiation Qs (heat absorbed by the ocean from incoming solar radiation), the net long-wave radiation Qb (heat lost by back radiation), the latent heat Qe (heat lost by evaporation) and the sensible heat Qc (the heat lost by convection and conduction).

$$Qi = Qs - (Qb + Qe + Qc)$$

### 2.3.3 Water transport through the borders of the box

To analyse the different water fluxes in the Ionian Sea, volume transport was calculated across four transects corresponding to the boundaries of the ION box. They were defined as the eastern (34-37°N and 20°E), northern (37°N and 16-20°E), western (34-37°N and 16°E) and southern (34°N and 16-20°E) transects. Monthly velocity components normal to each transect (u or v) were averaged within successive 100 m depth intervals from the surface to 1500 m depth. These values were then multiplied by the cross-sectional area of each depth layer (transect length × 100 m depth interval), to obtain the volume transport ($m^3/s$) through each 100 m layer of the transect, for each month. The transport is then expressed in Sverdrup (1 Sv = $10^6$ $m^3/s$). Because transport was averaged over the entire length of each transect, which extends over several hundred kilometers, local circulation features and spatial heterogeneity may be smoothed out. Consequently, the resulting transport estimates

should be interpreted as large-scale indicators of water exchange rather than precise representations of local flow patterns.

### 2.3.4 Deep currents and temperature and salinity from Argo data

To facilitate the plotting and the analysis of variables at different depths, we grouped the deep current data and the Argo float temperature/salinity data into 100 m depth bins (0-100 m, 100-200 m, etc.), following the same approach as in Section 2.3.3. The two types of data were treated differently within each bin, however: because Argo temperature and salinity measurements are sparse, all individual data points were retained and plotted on the map corresponding to their depth bin, whereas deep current data, derived from a continuous reanalysis grid rather than discrete in-situ points, were averaged over each 100 m interval before plotting. Since this study covers depths of approximately 1500 m, 15 bins of 100 m each represent a reasonable balance between vertical resolution and the number of maps to analyse.

# 3. Results

## 3.1 Warm and salinity anomalies in the Ionian Sea

The high temperature anomaly detected in the Ionian Sea using in-situ data from Argo floats is depicted in Figure 7a. In this figure, a warm signal composed of temperature anomalies exceeding 1°C warmer than the climatology is starting to be detected in April 2024 and lasts until at least December 2024. It extends from approximately 300 m to depths greater than 1000 meters. As displayed in Figure 7b, the high salinity anomalies (reaching ~0.4 psu) occur around the same depths and have the same time span. This warm and salty signal will be investigated in the next sections, with a characterization of the water masses present in the area, a study of the vertical and horizontal processes and an analysis of its monthly evolution.

## 3.2 Air-sea interactions

### 3.2.1 Heat fluxes

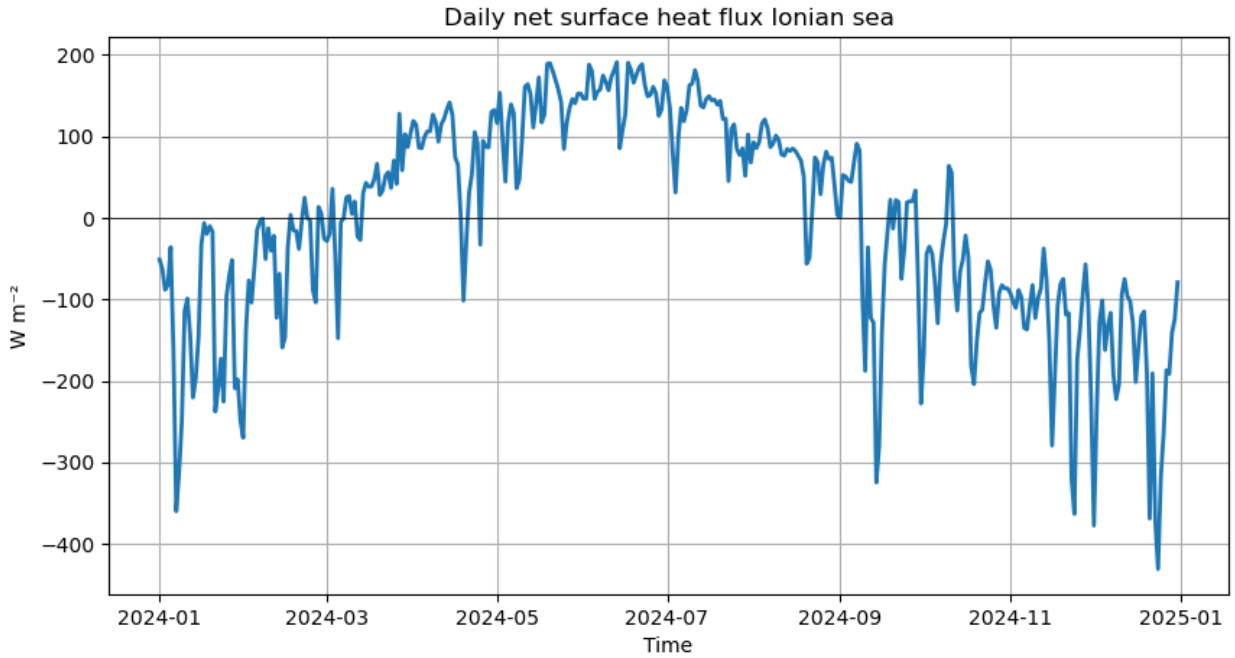


Figure 9: Weekly averaged net surface heat flux over the ION box in 2024.

The first step is to investigate the interactions between the atmosphere and the sea surface. The weekly net surface heat flux over the “ION” box is shown in Figure 9. In winter (Jan-Feb) and fall (Sep-Dec) months, the net total heat flux is negative,

meaning the surface is emitting heat (heat loss to the atmosphere), while in the spring and summer months, the net heat flux is positive, meaning the surface is absorbing heat from the atmosphere. The transition from net heat loss to net heat gain occurs in March and ends in September.

### 3.2.2 Winds

When winds blow across the sea surface, they exert a mechanical force on the water called wind stress. The wind stress generates turbulence that homogenizes the top few meters of the water column and deepens the mixed layer, mixing the warmer surface water with colder subsurface waters (Houpert et al., 2015; Babagolimatikolaei, 2025). To examine the evolution of wind velocity during 2024, the weekly wind speed average over the "ION" box was plotted (Figure 10). The wind speed average reaches its highest value at the beginning of January (7 m/s), then starts to decrease. Wind speed increases slightly in July and August before rising more markedly from October onwards.

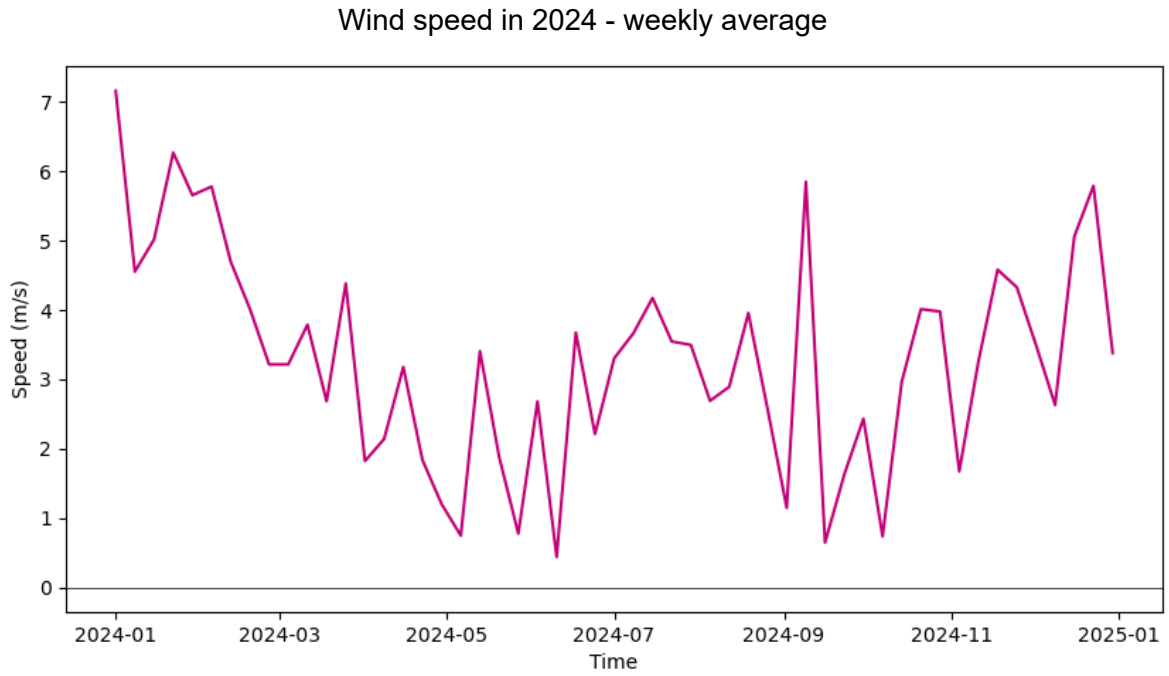


Figure 10: Weekly averaged wind velocities over the ION box in 2024.

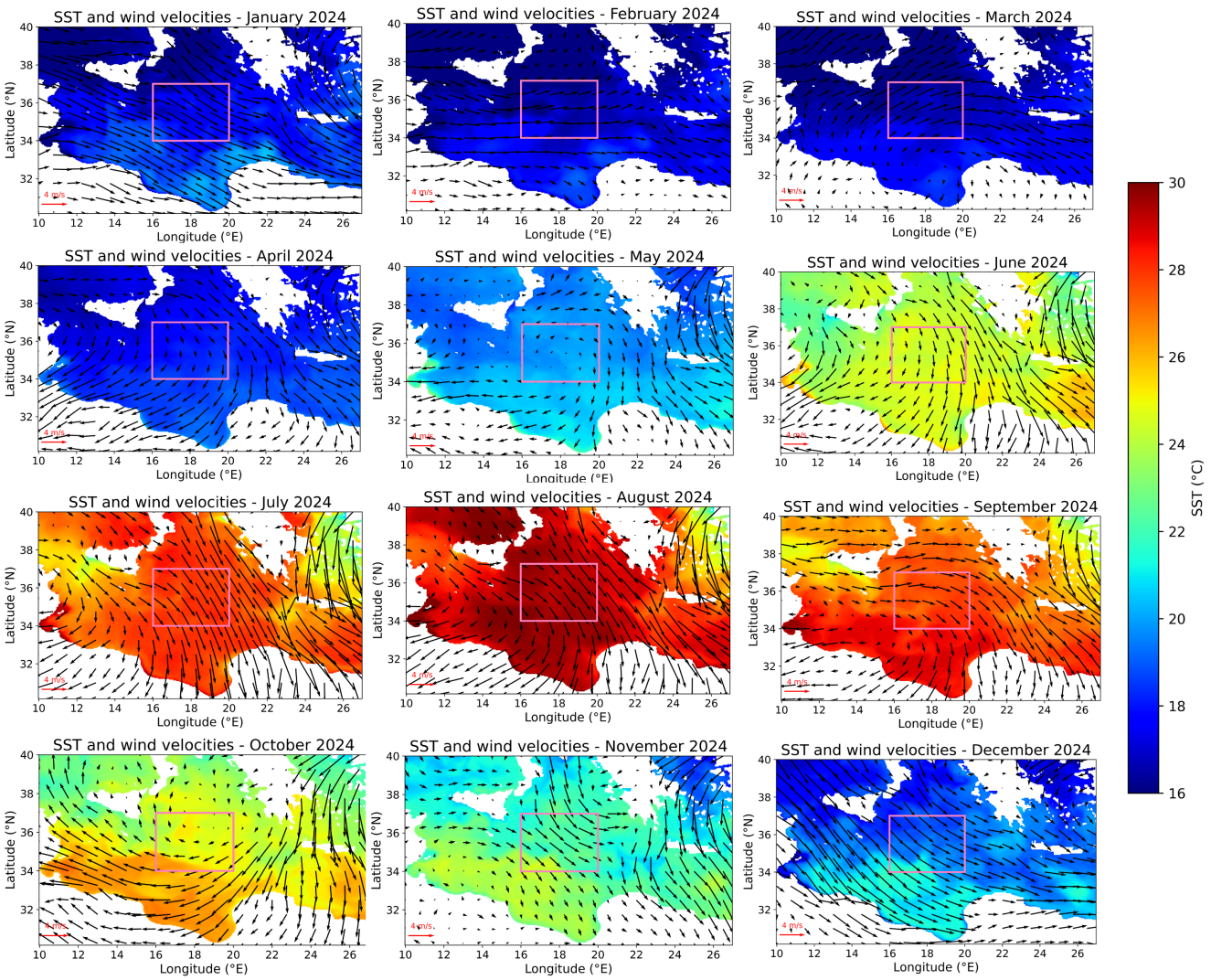


Figure 11: SST and wind velocities over the Ionian Sea in 2024. The study area's borders are highlighted in pink.

As shown in Figure 11, winds over the study area are predominantly eastward in January, February, and March 2024. In April, the wind direction shifts southward. During May, wind velocities decrease over the area and the circulation exhibits an anticyclonic rotation. From June onward, and until the end of the year, northwesterly winds dominate.

The sea surface temperatures are also displayed in this figure, showing a winter with temperatures hovering around 16°C in the study area and a very hot summer, especially in August, with temperatures reaching 30°C. There are no particular hot spots appearing in the study area during the first months of spring, nor during the rest of the year.

# 3.3 Sea surface processes: surface currents and absolute dynamic topography

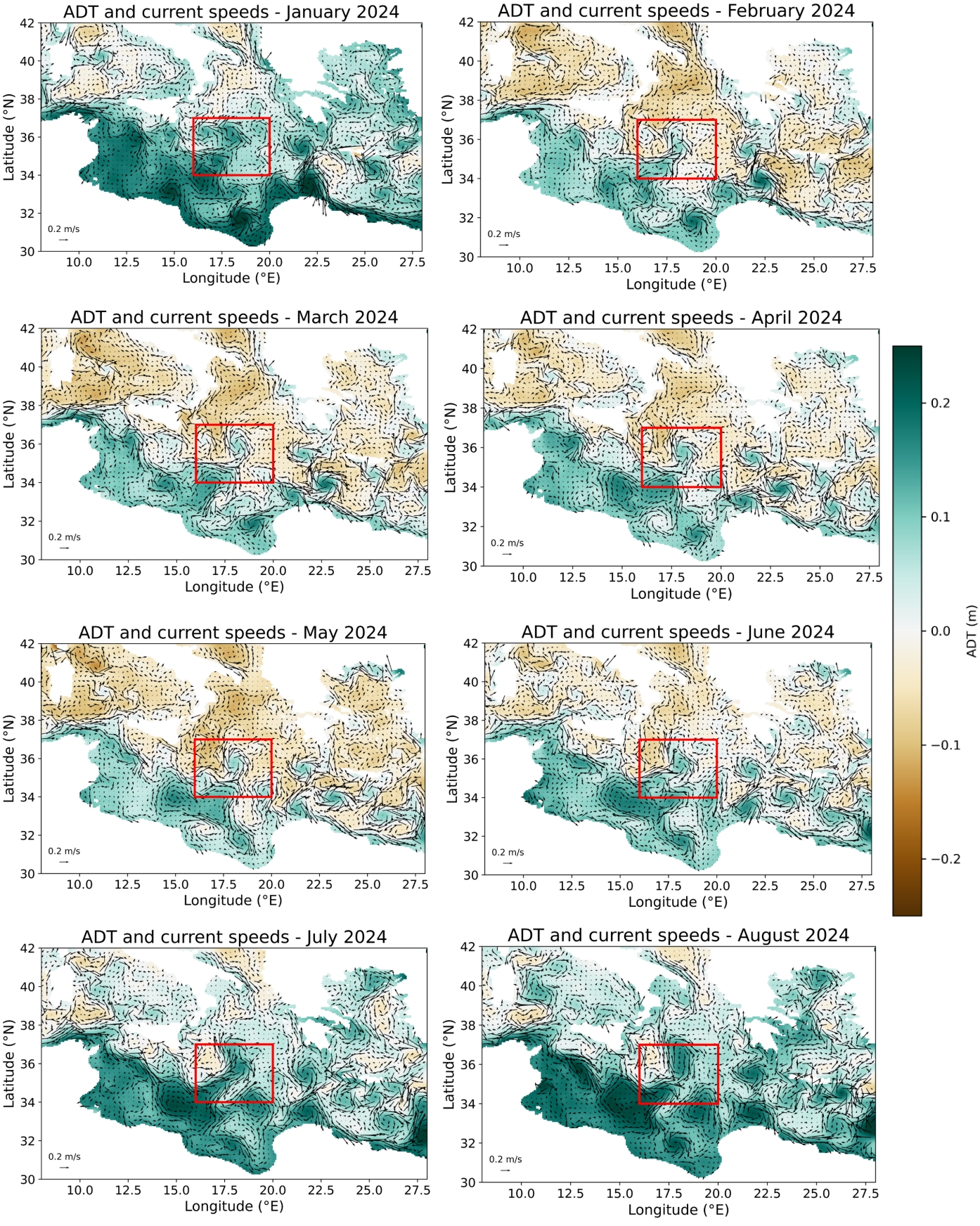

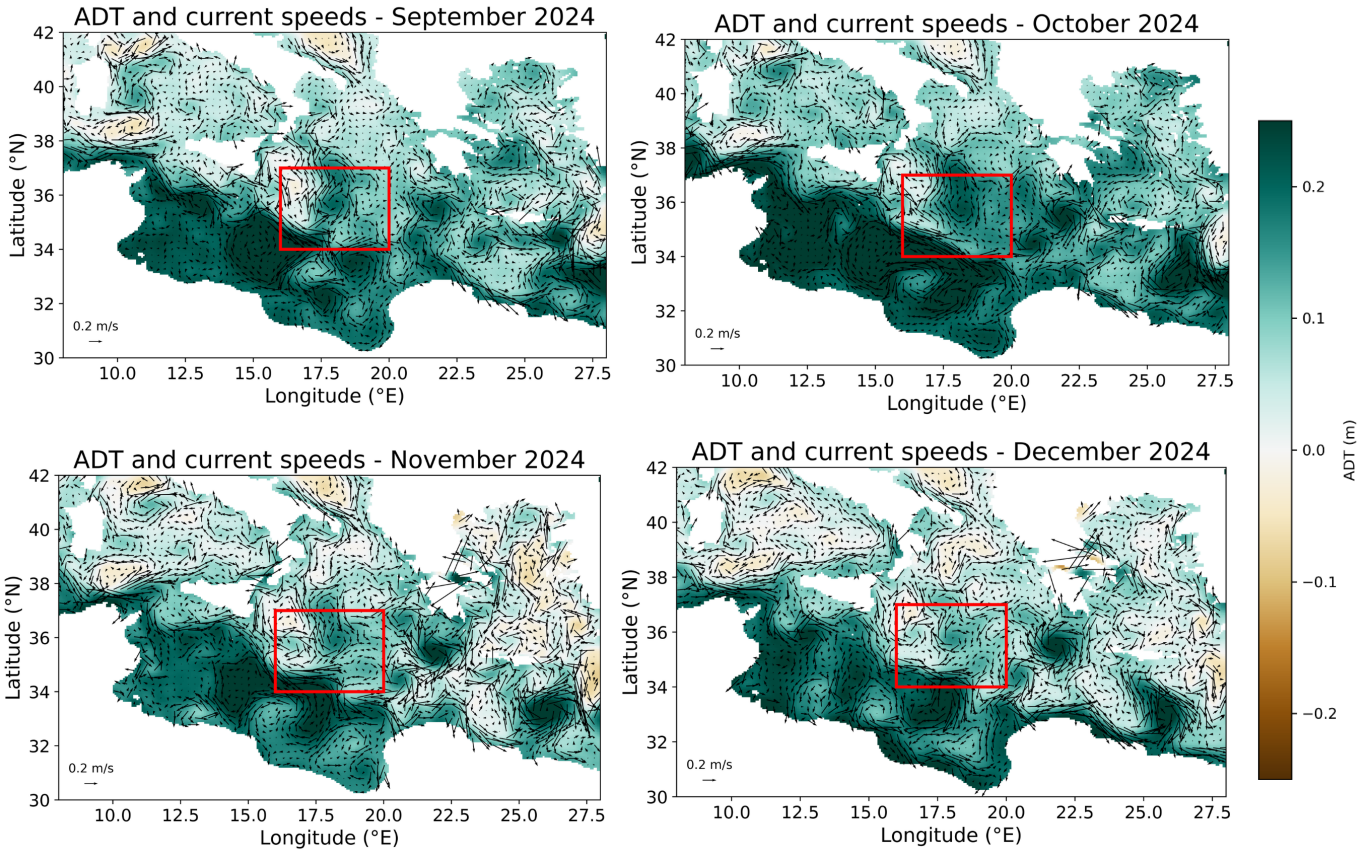


Figure 12: Absolute dynamic topography and current speeds over the Ionian Sea in 2024. The study area's borders are highlighted in red.

To further explore surface processes, the surface currents and the ADT were studied (Figure 12). From January to December 2024, a generally stable current can be observed, entering the basin from the west/southwest, forming an anticyclonic meander then exiting to the south. This anticyclonic gyre is quite pronounced during most months of 2024 and remains centered around the coordinates 36°N and 18°E. The gyre has a positive elevation, going from 0.05 up to more than 0.2 meters, which is indeed the case in high-pressure systems. Overall, the south of the Ionian basin has a positive ADT throughout the year and the north a negative one.

# 3.4 Deep currents

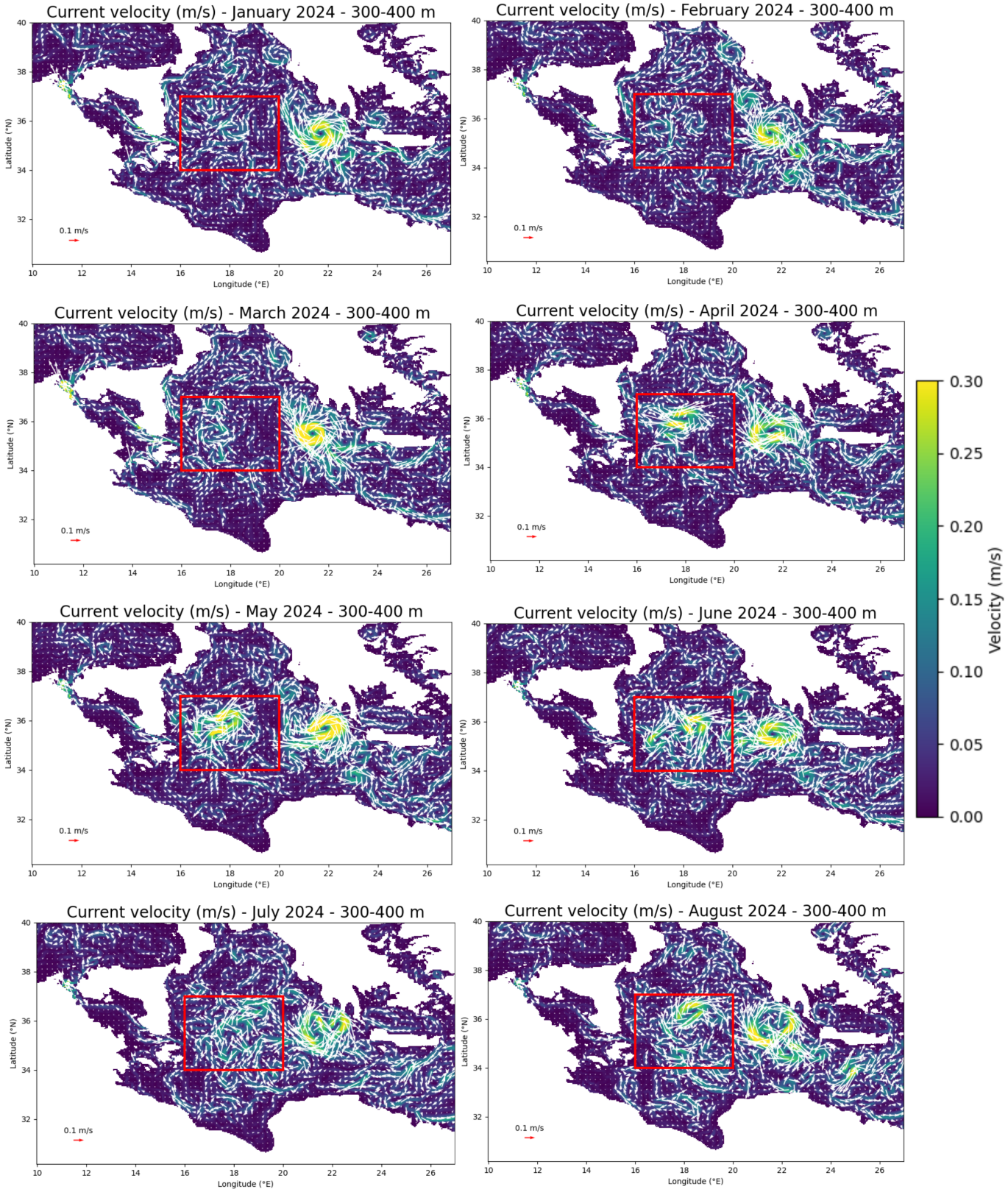

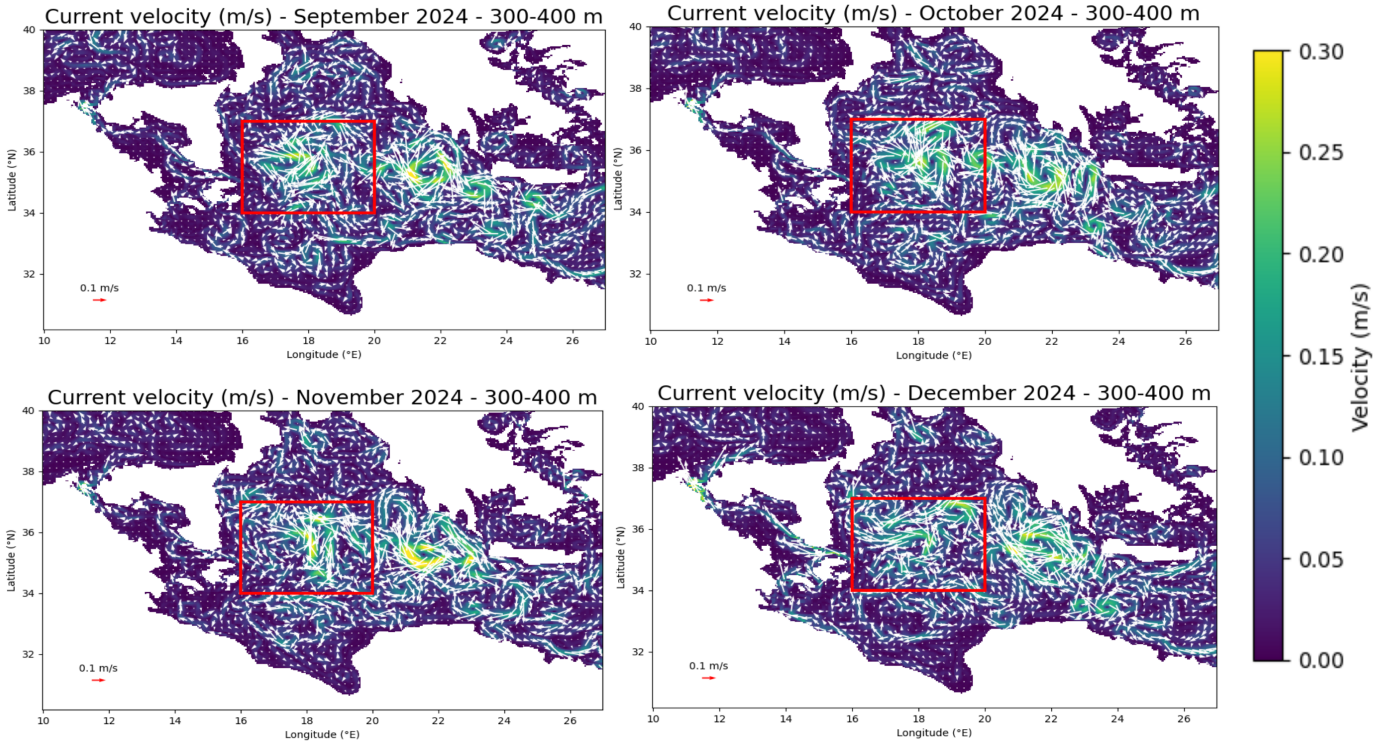


Figure 13: current velocities averaged between 300-400m over the Ionian Sea in 2024. The study area's borders are highlighted in red.

The anticyclonic gyre of the central Ionian Sea appears to have a vertical extension up to about 700m (Figure S1 in the Appendix). As shown in Figure 13, the anticyclone starts to be visible in April, around the same coordinates as at the surface. It shows high velocities (up to 0.3 m/s between 300-400 meters depth), similar to those of the PG, and it remains fairly pronounced through the end of the year, with some fluctuations during certain months. Together with the PG, this gyre appears to be one of the dominant features of the basin's velocity field.

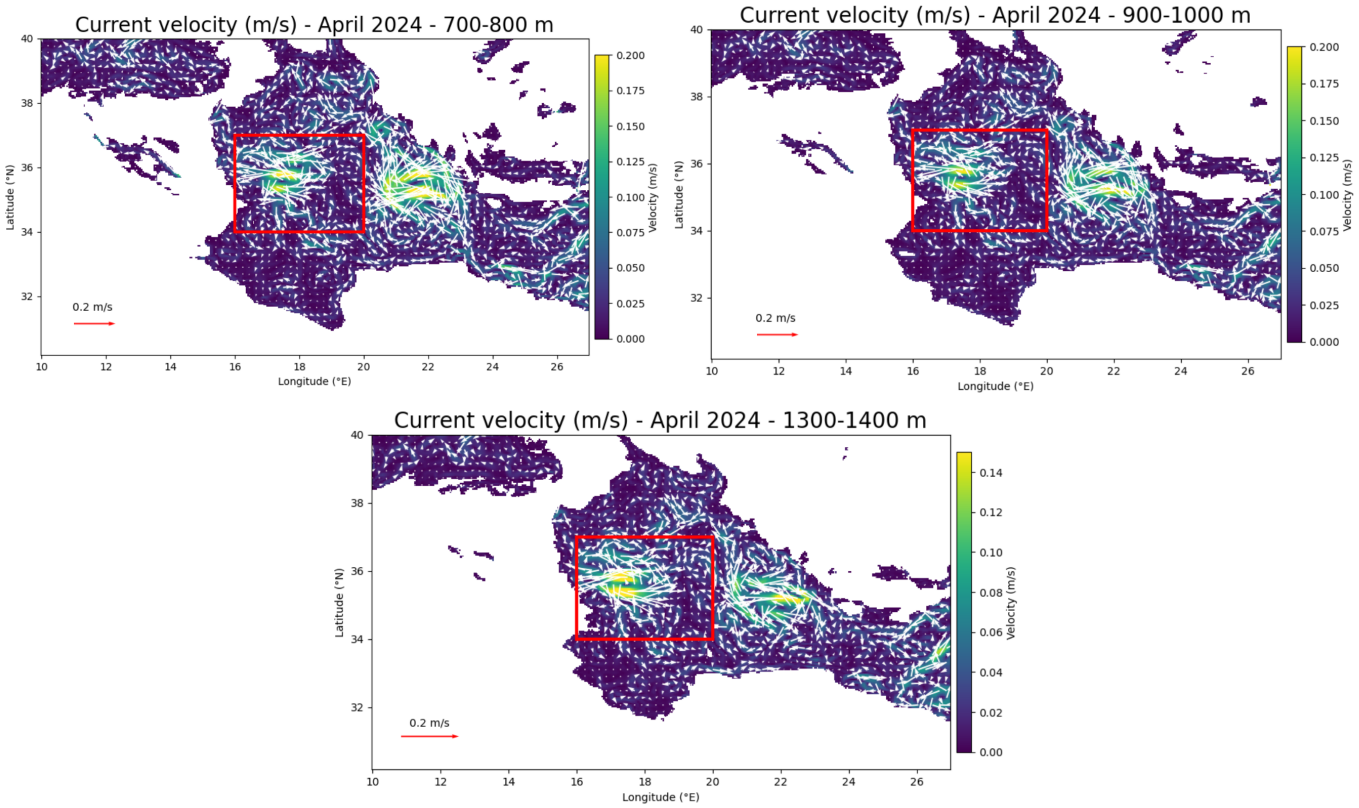


Figure 14: current velocities in April 2024 over the Ionian Sea at different depths (700-800m, 900-1000m, 1300-1400m). The study area's borders are highlighted in red. Note that the scales are different in every figure.

Below 700 meters depth, the anticyclonic rotation becomes less distinct and, at greater depths, the circulation pattern appears to become cyclonic (Figure 14). This cyclonic system also lasts until the end of 2024. Velocities reach approximately 0.2 m/s between 700-800 and 900-1000 meters depth, whereas they remain around 0.15 m/s between 1300 and 1400 meters.

## 3.5 Transport

In order to analyse the movement of the different water masses through the study area, the water transport through four transects delineating the area was investigated. To understand where this hot and salty water recorded in the study area in 2024 could have come from, we focused particularly on inflowing water during the month preceding the onset of the warm anomaly, i.e. in March. In March 2024, the flux through the eastern transect of the ION box changes direction and becomes negative, indicating an inward transport (Figure 15a). This inflow reaches values exceeding 0.3 Sv around 300 meters depth, and lasts until June, when the flux changes direction

again and becomes outward. In the uppermost layer, the inflow develops later, in April and May. Between 500-600m, the inflow is lower (0.2 Sv) and is starting later as well, but persists until July. Deeper, between 1000-1100m, the inflow peaks in May, reaches less than 0.1 Sv and stops in the middle of July.

After June, the strongest inflow occurs through the southern transect, reaching 0.6 Sv in December (Figure 15b). There is no inflow in the uppermost layer, and the deeper layers are following the same pattern as the eastern transect's, with the flux becoming inward later in the year and with lower values. No significant inflows are observed through the northern and western transects during the spring of 2024 (Figure 15c and d).




Figure 15: Water flux through the eastern transect of the Ionian box (A), the southern transect (B), the northern transect (C), and the western transect (D). The mentions "in" and "out" are indicating if the water is inflowing or outflowing the ION box.

In order to examine the possible link between the water masses arriving in the study area from the east and the PG, we examined the water transport through a transect closer to the PG (Figure 8). The transport through this transect remains markedly negative throughout 2023 and the first part of 2024, indicating a persistent westward flow, feeding into the ION box through its eastern transect. It reaches ~0.4 Sv between 200-300 m in May 2024 and >0.7 Sv between 0-100m in June 2024 (Figure 16).

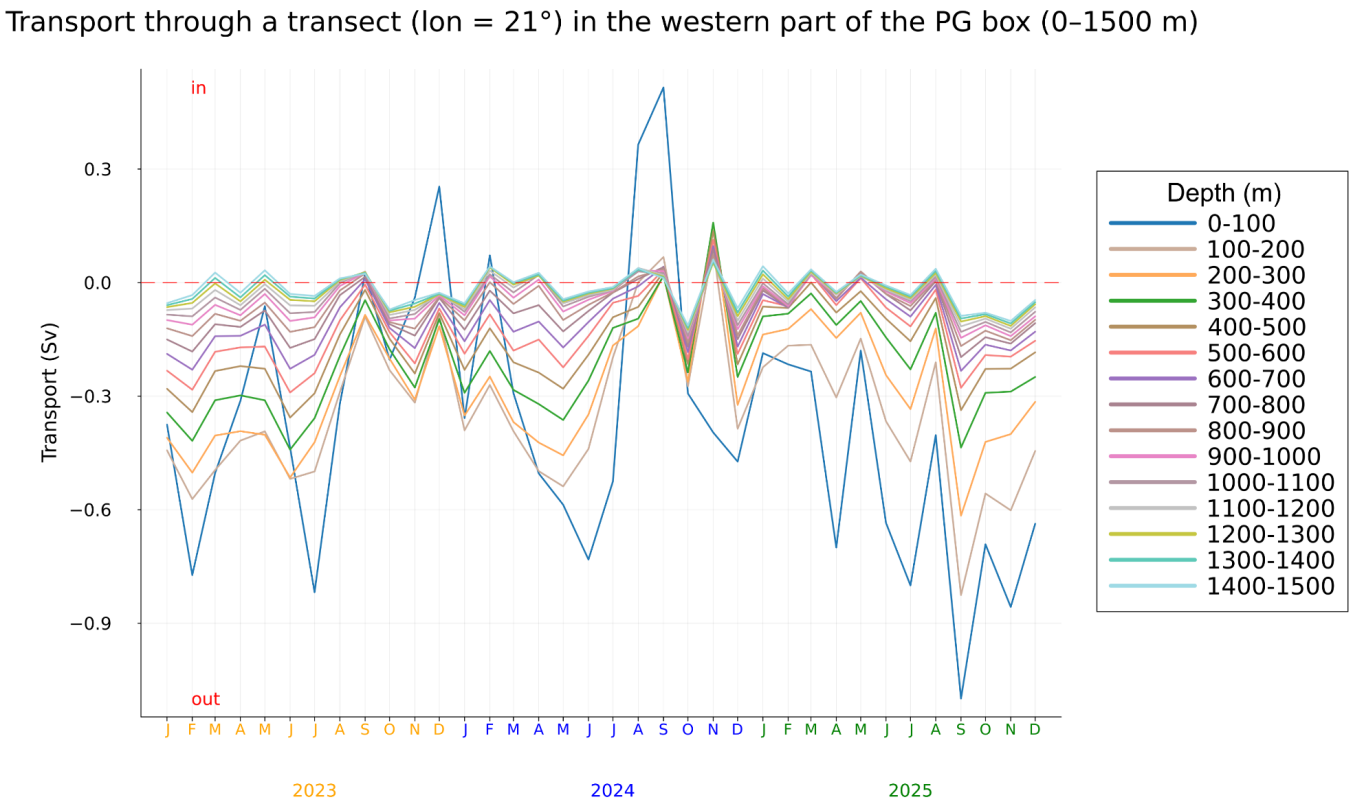


Figure 16: Water flux through a transect located in the western part of the PG box, at 21°E (the yellow dotted line in Figure 8). The negative values represent a flow directed to the West, meaning it's flowing "out" of the PG (in the direction of the ION box).

## 3.6 Temperature and salinity derived from Argo floats data

Maps of temperatures and salinities measurements collected by Argo floats were produced with the aim of spatially identifying the different water masses involved in the dynamic of the study area, analysing their temporal evolution and investigating potential connections between the waters present within the study area and those in surrounding regions. The temperature maps (Figure 17) show that most of the temperatures recorded in the study area range between 14°C and 15°C at depths of

500-600 meters. However, starting in March, temperatures of 14-15°C persist along the boundaries of the study area, whereas higher temperatures (15-16°C) are observed around 36°N and 18°E, corresponding to the center of the anticyclonic gyre in the Ionian Sea (Figures 12 and 13). This warm signal persists until the end of the year. In the salinity maps (Figure 18), most measurements within the study area range between 38.8 and 39.0 psu at depths of 500-600 m. Elevated salinities (39.1-39.2 psu) are observed over the same period and at the same location as the warm signal, indicating a spatial and temporal coincidence between the two features.

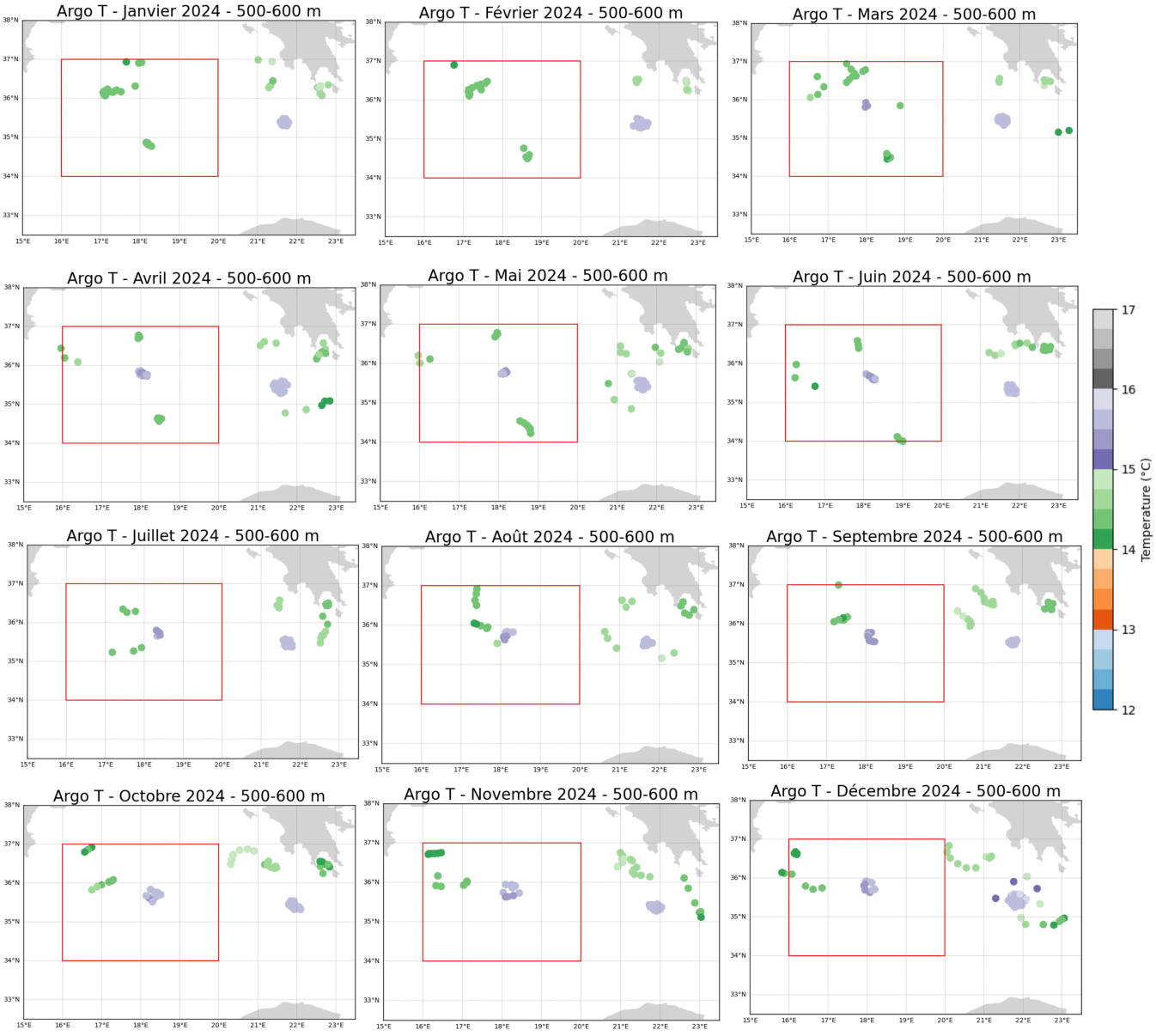


Figure 17: Temperatures measured by Argo floats between 500-600 m in 2024 in the Ionian Sea. The study area's borders are highlighted in red.

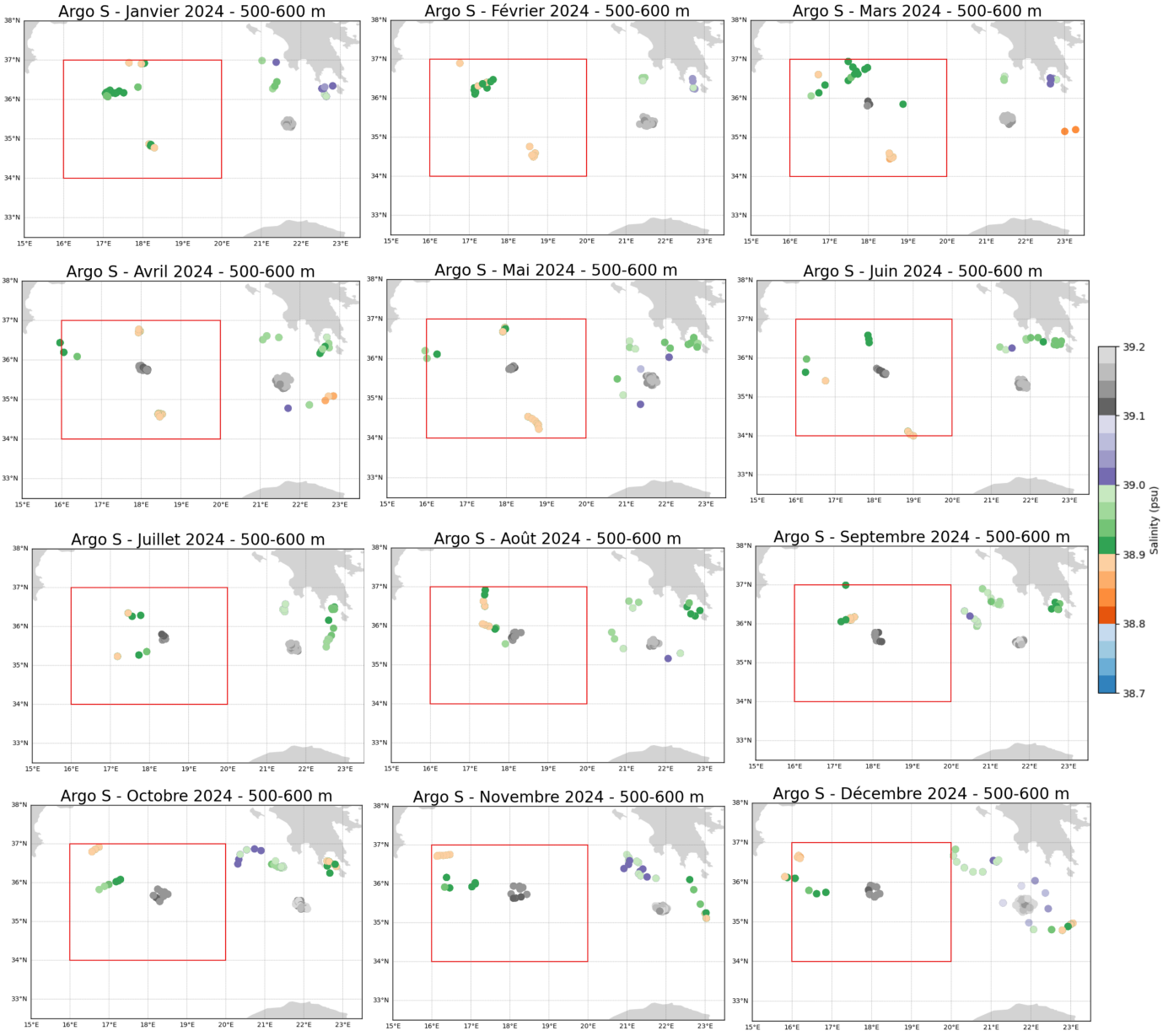


Figure 18: Salinities measured by Argo floats between 500-600 m in 2024 in the Ionian Sea. The study area's borders are highlighted in red.

In the uppermost layers, no particularly warm and/or high saline signal is detected (Figures S2 and S3 in the Appendix). This abnormally warm and salty water mass actually begins to be detected at a depth of 300 meters and extends down to 1500 meters. At 800 meters, its temperature decreases to ~15°C and its salinity to 38.9-39 psu (Figures S4 and S5 in the Appendix). At 1400 meters, it has a temperature of ~14°C and a salinity of ~38.8 psu (Figures S6 and S7 in the Appendix).

Even though the data are sparse, significant spatial variations in temperature and salinity are observed around the study area (Figures 17 and 18). Temperatures

of 14-15°C and salinities of 38.9-39.1 psu are recorded along the Greek coast. Water masses with the same temperatures but with salinities of 38.8-38.9 psu are reported along the southern coast of Crete. A stable formation, corresponding to the PG (35.5°N and 22°E), is recorded throughout the year with temperatures of 14-16°C and salinities of 39.1-39.2 psu (between 300 m and 1100 m deep). In the uppermost layer, the entire region along the Greek coast, including the PG, exhibits temperatures of at least 17°C and salinities of 39.1-39.2 psu throughout 2024 (Figures S2 and S3 in the Appendix). Deeper than 1100 m, temperatures of ~14°C and salinities of ~38.8 psu are observed in the PG, which also remains stable throughout the year (Figures S6 and S7 in the Appendix).

# 4. Discussion

In this paragraph, we examine and discuss the possible origins and mechanisms sustaining the warm and saline anomaly observed in the intermediate layers of the Ionian Sea throughout 2024. We first assess whether local atmospheric forcing could account for the signal (4.1), before evaluating the reliability of the in-situ and reanalysis datasets used to characterize it (4.2). We then investigate the sub-basin scale gyre co-located with the anomaly: we examine its vertical structure and the dynamical mechanisms that may explain both the arrival and the persistence of the warm and saline waters in the study area (4.3-4.4). Building on the temperature and salinity characteristics of the anomaly, we propose a possible advection pathway connecting the PG and the Levantine Basin to the central Ionian Sea (4.5-4.6). Finally, we place these local observations within the broader context of the ongoing warming and salinification trend affecting the Ionian Sea (4.7).

## 4.1 Atmospheric processes: heat fluxes and wind

Considering that MHWs are first recorded at the ocean surface and eventually deepen over time (Darmaraki et al., 2019; Dayan et al., 2023; Pirro et al., 2024), the first processes that were investigated are the surface processes, more specifically the interactions between the sea surface and the atmosphere. Variations in the net heat flux during 2024 (Figure 9) seem to simply follow a seasonal cycle and correspond to what is documented in the literature (Song and Yu, 2017). No anomaly of the net heat flux compared to that general seasonal cycle is to be noted in our results.

Wind speed and direction can have a significant impact on the sea, not only on the surface but in the subsurface layers too. When winds blow across the sea surface, they exert a mechanical force on the water called wind stress. The wind stress generates turbulence that homogenizes the top few meters of the water column and deepens the mixed layer, mixing the warmer surface water with colder subsurface waters (Houpert et al., 2015; Babagolimatikolaei, 2025). The variation of the wind speed during 2024 (Figure 10) also follows a seasonal cycle, decreasing in the warmer months thus inducing the restratification of the water column, and increasing in winter, in association with a deepened mixed layer (Houpert et al., 2015; Babagolimatikolaei,

2025). As for the wind circulation (Figure 11), the 2024 wind regime over the Ionian Sea is broadly consistent with the climatological pattern observed in previous years (1979-2014 climatology; Soukissian et al., 2018) characterized by predominantly southeastward winds throughout most of the year and eastward winds during early winter. Nevertheless, a noticeable deviation is observed, with the shift from eastward to southeastward winds occurring in April rather than January. This shift occurs at approximately the same time the anomaly starts to be recorded, raising the possibility that the change in wind regime contributed to reinforcing anticyclonic circulation in the upper layers. However, wind forcing primarily affects the surface and near-surface layers, whereas the anticyclonic circulation and the warm and saline anomaly are still (or only, in the case of the anomaly) pronounced at higher depths (Section 4.3.2). This vertical distribution suggests that the wind shift alone is unlikely to account for the gyre and the anomaly, although it may have reinforced it at the surface.

## 4.2 Characterizing the anomaly: in-situ evidence and data limitations

In Figures 17 and 18, the temperature and salinities recorded in the study area vary spatially. A hot and salty signal is reported from March to the end of 2024, at 36°N and 18°E, and temperatures and salinities are lower in the areas surrounding this restricted zone. With the examination of Table 2 and the supplementary Figure S8, we can connect these recordings of warm and salty water masses with one Argo float that was launched on March 29, 2024 and that remains at approximately the same location throughout the year (WMO 6990629). This signal occurs within the same time and depth ranges as the anomaly detected in Figure 7. Since both are derived from the same Argo float dataset, this consistency confirms that the box-averaged anomaly shown in Figure 7 originates specifically from this localized feature, rather than from a more diffuse signal elsewhere in the box. The apparent onset of the signal in April rather than March in Figure 7 is due to the late deployment of the float occurring on March 29, 2024. Because no float was covering this restricted zone since January 2024 (Figures 17 and 18), the exact timing of the arrival of this water mass remains uncertain: the water mass may have reached the area before 29 March 2024, but the available data are insufficient to determine this with confidence.

## 4.3 Structure and dynamics of the gyre

### 4.3.1 At the surface

The anticyclonic gyre visible on Figure 12 is located near the same coordinates as the subsurface warm and saline anomaly detected by the Argo floats (Figures 17 and 18). Deep-current maps reconstructed with the Copernicus Marine Physics Reanalysis (Figure 13) also display a gyre centered at the same coordinates. An anticyclonic circulation at the surface around the coordinates 36°N and 18°E appears to have been present since 2017 (see Figure S9 in the Appendix). Specifically, Figure 12 displays a surface current entering the study area from the southwest, following an anticyclonic meander before exiting southward. This circulation corresponds to a modified pathway of the MIJ (Dechenne et al., 2026), rather than the direct eastward route towards the Levantine Basin commonly reported in the literature (Pinardi et al., 2015; Menna et al., 2019; Liu et al., 2022; Civitarese et al., 2023). Dechenne et al. (2026) associated this new circulation pattern with two vortices, visible since 2017 and stable since 2020: one cyclonic and one anticyclonic, located at 16°E and 18°E respectively, and both at 36°N. This anticyclonic vortex is likely the same feature identified in the present study. At the surface, the cyclonic gyre entrains cold Adriatic waters, while the anticyclone advects relatively warm waters from the southern Ionian Sea, generating a frontal zone between the two water masses. Our results show that in 2024, only the anticyclonic gyre is present. Since the gyre was already present before 2020, the strengthening observed after 2020 may reflect an intensification of a pre-existing circulation feature rather than the formation of a new one (Dechenne et al., 2026). Some of the possible causes may be the strengthening of the MIJ caused by the NIG as demonstrated by Menna et al. (2019) or the enhancing of the front caused by an intensification of the Ionian temperature gradient, which increases the part of the MIJ flowing in the direction of the pre-existent gyres (Dechenne et al., 2026). Dechenne et al. (2026) showed that the gyre strengthened during the second half of the year (autumn/early winter) during the 2013-2022 period. In contrast, our results show that in 2024, the strengthening occurred much earlier, during spring.

Figure 11 shows that at the surface, no particular hot spot is to be noticed in the study area, in April nor in the following months. The summer months, however, show particularly warm temperatures over the whole Ionian Sea, a sign that the 2022

MHW event was still ongoing. This basin-wide warming is not specific to the anticyclonic gyre, however: the figure demonstrates that at the surface, the water is not particularly warmer in the zone of the anticyclone than elsewhere in the basin. High temperatures and salinities are in fact recorded from 300 m to 1500 m deep (Figures 17 and 18). This coincidence in the localisation of the warm and saline anomaly and the anticyclonic gyre, together with its apparent strengthening after 2020, suggests that the gyre may play a role in shaping the vertical structure and persistence of the anomaly. We further examine this hypothesis in the following section, through the analysis of the gyre's vertical structure.

### 4.3.2 In deeper layers

In Figures 12 and 13, we observe that the vortex remains anticyclonic down to approximately 700 m depth. In the Northern Hemisphere, downwelling processes occur in anticyclonic eddies, whereas cyclonic eddies promote upwellings. These vertical motions, commonly referred to as *eddy pumping*, result from variations in the rotational strength of mesoscale eddies. As a consequence, anticyclonic eddies are often characterized by warm cores, as warm surface waters are displaced downward into the water column (Ni et al., 2023). However, the warm and saline anomaly observed between 300 and 1000 m depth is unlikely to be caused by downwelling of local surface waters, since surface salinity (~38.7 psu; Figure S3 in the Appendix) is substantially lower than the salinity measured within the anomaly (~39.2 psu between 500-600 m depth; Figure 18). If the anomaly resulted primarily from the downward transport of local surface waters, comparable salinity values would be expected. The marked salinity difference therefore suggests that the anomalous waters originate from a distinct water mass rather than from local surface waters subducted within the gyre. These observations support the hypothesis that the warm and saline waters were advected into the study area from adjacent regions.

## 4.4 Onset and persistence of the anomaly

The transport analysis described in Section 3.5 indicates that the strongest inflows into the ION box occurred through the eastern boundary (Figure 15a) in conjunction with the starting of the temperature anomaly registered in March-April 2024. The study of an additional transect located within the PG box confirms that

during the same period, water masses were strongly transported toward the ION box (Figure 16). From June onward, transport through the southern boundary became increasingly important and remained directed into the study area until the end of the year (Figure 15b). Together with the temperature and salinity characteristics identified from Argo observations (Section 3.6), these results support the hypothesis that the anomaly was initially supplied by waters originating from the PG region, at all depths, and may have been subsequently maintained by continued inflows through the southern boundary, between ~200-1500 m depth.

The reconstructed deep circulation also provides a possible explanation for the remarkable persistence of the warm and saline water mass throughout 2024. In Figure 14, at a depth of 700 meters, the circulation exhibits an anticyclonic pattern, while below this depth, down to around 1500 meters, the rotation reverses and becomes cyclonic. As discussed previously, cyclonic eddies are generally associated with water upwellings, whereas anticyclonic eddies tend to favor downwelling. The vertical stacking of an anticyclonic circulation overlying a deeper cyclonic circulation may therefore limit vertical exchanges and contribute to a situation in which the warm and saline water mass would become trapped between the two formations.

### 4.4.1 Vertical structure and candidate dynamical mechanisms: the heton framework and vorticity conservation

Structures composed of two counter-rotating eddies can significantly alter vertical mass transport; they can transport and maintain temperature and salinity anomalies more effectively than a single eddy. These configurations can be modelled as hetons, which are idealized structures that have pairs of superimposed vortices in a simplified two-layer ocean (one in the upper layer, one in the lower layer), with opposite rotations (Hogg and Stommel, 1985). In such a framework, the heton traps a volume of water between its vortices, and this mass remains coherent over long periods of time. This trapping property is particularly pronounced in the limiting case where the horizontal separation between vortices tends to zero. While the original authors defined hetons as a tilted baroclinic pair (Hogg and Stommel, 1985), a definition of a heton that is perfectly vertically aligned (has zero horizontal separation) was introduced by Sivakumar and Weiss (2022), describing it as stationary; there is thus no net advection of fluid relative to the heton. In the real ocean, however, this

perfect symmetry almost never exists: frictional effects, large-scale gradients, non-uniform vertical stratification, planetary vorticity gradient (β-effect) and baroclinic instabilities disrupt this structure and allow for slow propagation and net transport (Sivakumar and Weiss, 2022). Since the observed structure is only quasi-aligned rather than perfectly vertical, it likely operates close to this near-stationary regime: advection relative to the heton remains weak but non-zero, which would explain both the extended persistence of the warm and saline water mass throughout 2024 and its eventual erosion or displacement over time.

An alternative hypothesis is that the observed vertical circulation structure may itself result from the warm anomaly. An increase in temperature reduces the density of water, leading to thermal expansion of the upper water column. If the layer thickness (h) is increasing, the relative vorticity (ζ) also has to increase to conserve the potential vorticity (q; Cushman-Roisin and Beckers, 2006):

$$q = \frac{f + \zeta}{h}$$, where f is the Coriolis parameter.

In an idealized two-layer system, if one layer thickens because of thermal expansion, the overlaying/underlying layer, on the contrary, may contract. Such vertical adjustments may generate opposite potential-vorticity anomalies in adjacent layers and favor the development of a vertically coupled baroclinic circulation (Hoskins et al., 1985). The anticyclonic circulation observed in the intermediate layers and the cyclonic circulation below may therefore reflect a baroclinic response to the redistribution of heat rather than two independent gyres. This mechanism could also possibly explain why the gyre strengthened in the spring 2024, rather than during autumn as observed in previous years (see Section 4.3.1).

An important question raised by these observations is whether the baroclinic structure preconditioned the trapping of the warm and saline water mass, or whether the warm anomaly itself contributed to the development of the observed circulation by inducing adjustments in the relative vorticity. Addressing this question would require additional diagnostics, including computation of the potential vorticity, evolution of the thickness of isopycnal layers, available potential energy or diagnosis of baroclinic instability. These two mechanisms are, however, not mutually exclusive. A pre-existing baroclinic circulation may initially have favored the trapping of the warm and saline

water mass, while the resulting thermohaline anomaly may in turn have modified the local potential-vorticity distribution and reinforced the vertical circulation structure. Given the limited coverage of in-situ observations, a hydrodynamic model of the area could help disentangle the relative contributions of the pre-existing circulation and the thermohaline anomaly to the development and persistence of the gyre.

## 4.5 Characteristics of the water masses

The temperature and salinity characteristics identified from Argo observations (Figures 17 and 18) are very similar in the gyre where the anomaly was recorded and in the PG, at intermediate depths. Indeed, both regions exhibit, throughout the year, temperatures of 15-16°C and salinities of 39.1-39.2 psu between 300 and 800 m depth. Below this depth, water mass properties start to differ between the two formations; the PG displays temperatures approximately 1°C higher than the gyre in the ION box: at 800-900 m, temperatures range from 15-16°C in the PG compared with 14-15°C in the ION box (Figure S4 in the Appendix), while at 1400-1500 m, they range from 14°-15°C and 13°-14°C, respectively (Figure S6 in the Appendix). A similar pattern is observed for salinity, with values of 39.1-39.2 psu in the PG compared with 38.9-39.1 psu in the ION box at 800-900 m (Figure S5 in the Appendix), and 38.8-38.9 psu compared with 38.7-38.8 psu at 1400-1500 m (Figure S7 in the Appendix). The PG is usually filled with LSW of salinities exceeding 39.1 between 50-80 m, LIW of salinities 38.9-39.05 between 250 and 450 m and water of salinities of 38.85-38.9 between 800 and 1000 m (Menna et al., 2021). The salinities recorded during 2024 in the PG are thus higher than usual.

As explained previously, the center of the PG experiences downwelling processes driven by the anticyclonic dynamics of the gyre. From 2022 until 2024, these downwelling processes, combined with persistent MHW conditions (see Section 1.3.3 and 1.3.4), likely contributed to pronounced positive temperature anomalies within the PG's intermediate and deep layers (Pirro et al., 2024). Indeed, the maximum recorded anomaly reached +0.4°C at 400 m in 2022, +1°C at 900 m in 2023, and +1.4°C at 900 m in 2024 (Figure 6). However, the high salinities observed at great depths in the PG are most likely not a direct consequence of the MHW but rather a characteristic feature of the PG (Menna et al., 2021) that may be further enhanced under MHW conditions, downwelling the LSW and LIW deeper than usual.

The similar temperature and salinity characteristics of the LSW and LIW waters in the PG and the waters observed within the ION box between 300 and 800 m depth suggest that the latter may possibly be of Levantine origins and may have transited through the PG. Below 800 m, the observed temperature and salinity characteristics may instead reflect a combination of southward-source waters entering through the southern transect and the upwelling associated with the cyclonic circulation. The Argo measurements shown in Figures 17 and 18 are, however, sparse, and the areas south, west and north of the Ionian basin are poorly sampled. This limited spatial coverage makes it difficult to compare the properties of water originating from these regions.

## 4.6 Water current into the central Ionian

The temperature and salinity characteristics derived from the Argo observations, together with the water transport analysis, are consistent with the hypothesis that waters of Levantine origin transited through the PG, where they may have undergone downwelling, before reaching the central Ionian Sea. The transport analysis suggests that these waters first entered the study area through the eastern boundary and subsequently through the southern boundary. Notably, no significant inflow was detected through the northern or western transects during 2024. To our knowledge, a pathway by which Levantine waters are advected westward from the PG towards the central Ionian Sea in the intermediate layers has not been explicitly described in the literature. However, this interpretation remains tentative, as the reconstructed current fields do not clearly reveal a persistent westward flow connecting the PG to the study area.

## 4.7 General warming and salinification of the Ionian Sea

Although the warm and saline anomaly identified in this study appears to be localized, it developed during a period of rapid warming and salinification of the Ionian Sea (Menna et al., 2026; Terzić and Vilibić, 2026). For instance, several salinity measurements exceeding 39 psu were observed in this study, values that were rarely reported in the Mediterranean before 2011. In particular, the period 2022-2024 was characterized by an abrupt intensification of the positive temperature and salinity trends in the Ionian Sea, especially in the intermediate and deep layers. This regional evolution is particularly evident in the vicinity of our study area. Indeed, in the sector

of the Ionian Sea encompassing our study area, the differences in annual median temperature between 2022 and 2024 reach approximately 1°C between 300 and 500 m, increasing to about 1.5°C at 700 m depth. Similarly, salinity differences are greatest at intermediate depths, reaching 0.21 psu at 500 m and 0.34 psu at 700 m. These anomalies are the most intense in the southern and southeastern Ionian Sea. The pronounced warming and salinification of the intermediate layers (300-1200 m) in 2022-2024 likely strengthened the density contrasts driving the BiOS, potentially preconditioning the basin for future regime shifts (Terzić and Vilibić, 2026).

Terzić and Vilibić (2026) proposed that anomalous surface forcing in winter 2021/2022 was a key driver in the process. Strong negative heat-flux anomalies and intensified wind stress likely increased vertical mixing and facilitated penetration of warm and saline LSW and LIW to greater depths. Over the subsequent two years, consistent with the propagation timescales of saline waters between Eastern Mediterranean basins, negative wind-stress anomalies, together with positive heat flux and excess evaporation over precipitation, may have reduced deep convection, allowing the warm and saline waters to persist at intermediate and deep depths while gradually spreading across the basin and towards the Western Mediterranean. Terzić and Vilibić (2026) further suggested that localized processes, such as downwelling associated with MIJ meanders or enhanced convection within the PG, may also have promoted the downward transport of heat and salt, although anomalies of comparable intensity had not previously been documented. Our observations are therefore consistent with the regional warming and salinity increase documented by Terzić and Vilibić (2026). However, they additionally suggest that, in the central Ionian Sea, horizontal advection of Levantine waters and circulation associated with the PG may also have contributed significantly to the development and persistence of the observed anomaly.

# 5. Conclusion and perspectives

In this work, the origin of a high temperature and salinity signal recorded in 2024 by Argo floats within an intermediate-deep layer (300-1000 m) in the central Ionian basin was investigated, along with the role of a quasi-permanent anticyclonic eddy present in the study area and the dynamics of adjacent basins. To that end, different atmospheric and oceanic variables were studied. No significant anomalies were identified in surface heat fluxes or wind speed. However, a shift in the wind direction over the study area was recorded at the same time as the apparent onset of the anomaly; this shift is nevertheless unlikely to account for the development of the gyre and the anomaly, although it may have contributed to reinforcing the surface circulation. The analysis of in-situ Argo floats measurements provided evidence for the vertical (300-1000 m) and horizontal confinement (around 36°N and 18°E), as well as the time span (from the end of March to at least December 2024), of the anomalous water mass. However, these estimates are subject to uncertainty because of the limited spatial and temporal coverage of in-situ observations.

The vertical structure of the circulation investigated with reanalysis data revealed an anticyclonic circulation extending down to approximately 700 m, below which the circulation reversed and became cyclonic. Although this mechanism cannot be confirmed from the available observations, the vertical opposition of the two circulation systems provides a plausible mechanism for limiting vertical exchange and maintaining the observed warm and salty anomaly. Further investigation is needed to understand the role of the dipole structure in the persistence of the warm and saline water mass in the study area. In particular, it remains unclear whether this baroclinic structure preconditioned the trapping of the water mass, or whether the warm anomaly itself contributed to the development of the observed circulation. At the surface, the gyre was clearly present during previous years (see Section 4.3.1), but it would be important to determine whether a similar vertical structure was already present during those earlier periods.

Finally, this work examined the possible provenance of the anomalous water mass. Highly saline water masses in the Mediterranean Sea typically originate from the Levantine basin (in the form of LIW or LSW; Lascaratos et al., 1993; Millot and

Taupier-Letage, 2005), and the temperature and salinity characteristics identified in this study (the LIW/LSW-like characteristics identified between 300 and 800 m) are consistent with such an origin. Transport analysis further suggests that these waters may have transited through the PG, which could have downwelled particularly warm water as a result of the 2022 MHW. This proposed pathway, however, remains hypothetical: the reconstructed current fields do not clearly reveal a persistent flow connecting the PG to the central Ionian Sea, and further work combining higher-resolution transport analysis and additional in-situ observations is needed to confirm this hypothesis.

Our results should be considered in the context of persistent positive trends in temperature and salinity in the Ionian and Mediterranean Seas, which may progressively alter regional climatology (Menna et al., 2026; Terzić and Vilibić, 2026). Rising temperatures and shifting stratification patterns have also been associated with declining biomass in the Ionian Sea and in other regions of the Mediterranean (Reale et al., 2022). This study highlights the potential role of remote advection and gyre dynamics in contributing to the persistence of subsurface warm and saline anomalies in the Mediterranean, an aspect that may deserve greater consideration in future monitoring and MHW detection efforts, which currently focus predominantly on surface signals. The cascading effects of MHWs therefore warrant further investigation, particularly given that they can persist long after the surface anomaly has dissipated (Bonino et al., 2025). In the Ionian Sea, more investigations about the gyre and the anomaly identified in this study would help clarify the potential feedback between thermohaline anomalies and circulation, as anomalously warm and saline waters may act both as a cause and a consequence of changes in regional circulation.

# References


Ali, E., Cramer, W., Carnicer, J., Georgopoulou, E., Hilmi, N. J. M., Le Cozannet, G., Lionello, P. 2023. Cross-chapter paper 4: Mediterranean Region, in: Pörtner, H.-O., Roberts, D.C., Tignor, M., Poloczanska, E. S., Mintenbeck, K., Alegría, A., Craig, M., Langsdorf, S., Löschke, S., Möller, V., Okem, A., Rama, B. (Eds.) Climate Change 2022: Impacts, Adaptation and Vulnerability. Contribution of Working Group II to the Sixth Assessment Report of the Intergovernmental Panel on Climate Change. Cambridge University Press, Cambridge, UK and New York, NY, USA, 2233-2272. https://doi.org/10.1017/9781009325844.021

Androulidakis, Y. S., Krestenitis, Y. N. 2022. Sea surface temperature variability and marine heat waves over the Aegean, Ionian, and Cretan Seas from 2008-2021. J. Mar. Sci. Eng. 10, 42. https://doi.org/10.3390/jmse10010042

Astraldi, M., Balopoulos, S., Candela, J., Font, J., Gačić, M., Gasparini, G. P., Manca, B., Theocharis, A., Tintoré, J. 1999. The role of straits and channels in understanding the characteristics of Mediterranean circulation. Prog. Oceanogr. 44, 65-108. https://doi.org/10.1016/S0079-6611(99)00021-X

Astraldi, M., Gasparini, G., Vetrano, A., Vignudelli, S. 2002. Hydrographic characteristics and interannual variability of water masses in the central Mediterranean: a sensitivity test for long-term changes in the Mediterranean Sea. Deep Sea Res. Part I 49, 661-680. https://doi.org/10.1016/S0967-0637(01)00059-0

Babagolimatikolaei, J. 2025. Three decades of Mediterranean mixed layer depth change: basin trends and regional contrasts. Front. Mar. Sci. 12, 1699007. https://doi.org/10.3389/fmars.2025.1699007

Bakun, A., Agostini, V. N. 2001. Seasonal patterns of wind-induced upwelling/downwelling in the Mediterranean Sea. Sci. Mar. 65, 243-257. https://doi.org/10.3989/scimar.2001.65n3243

Ballarotta, M., Pujol, M.-I., SL-TAC team. 2025. Quality Information Document. Sea Level TAC - DUACS products. E.U. Copernicus Marine Service Information (CMEMS).

Batistić, M., Garić, R., Molinero, J. 2014. Interannual variations in Adriatic Sea zooplankton mirror shifts in circulation regimes in the Ionian Sea. Clim. Res. 61, 231-240. https://doi.org/10.3354/cr01248

Béranger, K., Mortier, L., Crépon, M. 2005. Seasonal variability of water transports through the Straits of Gibraltar, Sicily and Corsica, derived from a high resolution model of the Mediterranean circulation. Prog. Oceanogr. 66, 341-364. https://doi.org/10.1016/j.pocean.2004.07.013

Bonino, G., McAdam, R., Athanasiadis, P., Cavicchia, L., Rodrigues, R. R., Scoccimarro, E., Tibaldi, S., Masina, S. 2025. Mediterranean summer marine heatwaves triggered by weaker winds under subtropical ridges. Nat. Geosci. 18, 848-853. https://doi.org/10.1038/s41561-025-01762-9

Civitarese, G., Gačić, M., Eusebi Borzelli, G. L., Lipizer, M. 2010. On the impact of the bimodal oscillating system (BiOS) on the biogeochemistry and biology of the Adriatic and Ionian Seas (eastern Mediterranean). Biogeosciences 7, 3987-3997. https://doi.org/10.5194/bg-7-3987-2010

Civitarese, G., Gačić, M., Batistić, M., Bensi, M., Cardin, V., Dulčić, J., Garić, R., Menna, M. 2023. The BiOS mechanism: History, theory, implications. Prog. Oceanogr. 216, 103056. https://doi.org/10.1016/j.pocean.2023.103056

Cushman-Roisin, B., Beckers, J.-M. 2006. Chapter 12.3. Potential vorticity, in: Introduction to Geophysical Fluid Dynamics: Physical and Numerical Aspects. Academic Press, 343-344. https://mcirano.ufba.br/ftp/books/cushman06/gfd2.pdf (accessed August 2026)

Darmaraki, S., Somot, S., Sevault, F., Nabat, P. 2019. Past variability of Mediterranean Sea marine heatwaves. Geophys. Res. Lett. 46, 9813-9823. https://doi.org/10.1029/2019GL082933

Darmaraki, S., Denaxa, D., Theodorou, I., Livanou, E., Rigatou, D., Raitsos, D., Stavrakidis-Zachou, O., Dimarchopoulou, D., Domino, G., McAdam, R., Organelli, E., Pitsouni, Z., Parasyris, A. 2024. Marine heatwaves in the Mediterranean sea: a literature review. Mediterr. Mar. Sci. 25, 586-620. https://doi.org/10.12681/mms.38392

Dayan, H., McAdam, R. O., Juza, M., Masina, S., Speich, S. 2023. Marine heat waves in the Mediterranean Sea: An assessment from the surface to the subsurface to meet national needs. Front. Mar. Sci. 10, 1045138. https://doi.org/10.3389/fmars.2023.1045138

Dechenne, A., Alvera-Azcárate, A., Beckers, J.-M., Barth, A. 2026. Mediterranean Sea surface currents obtained with a variational inverse method, insight on the central Ionian Sea. EGUsphere [preprint]. https://doi.org/10.5194/egusphere-2026-1627

Escudier, R., Clementi, E., Nigam, T., Aydogdu, A., Fini, E., Pistoia, J., Grandi, A., Miraglio, P. 2025. Quality Information Document. Mediterranean Sea Physics Reanalysis. E.U. Copernicus Marine Service Information (CMEMS).

EU Copernicus Climate Change Service Product 2026: ERA5 hourly data on single levels from 1940 to present. Climate Data Store (CDS). ECMWF [data set]. https://doi.org/10.24381/cds.adbb2d47

EU Copernicus Marine Service Product 2026a: Mediterranean Sea Physics Reanalysis. CMCC Foundation [data set]. https://doi.org/10.48670/mds-00375

EU Copernicus Marine Service Product 2026b: European Seas Gridded L4 Sea Surface Heights And Derived Variables Nrt. CLS [data set]. https://doi.org/10.48670/moi-00142

EU Copernicus Marine Service Product 2026c: Mediterranean Sea- In-Situ Near Real Time Observations. HCMR [data set]. https://doi.org/10.48670/moi-00044

Euro-Argo. 2026. Argo Fleet Monitoring. France. https://fleetmonitoring.euro-argo.eu/dashboard (accessed August 2026)

Eusebi Borzelli, G. L., Gačić, M., Cardin, V., Civitarese, G. 2009. Eastern Mediterranean Transient and reversal of the Ionian Sea circulation. Geophys. Res. Lett. 36, L15108. https://doi.org/10.1029/2009GL039261

Eusebi Borzelli, G. L., Napolitano, E., Carillo, A., Struglia, M., Palma, M., Iacono, R. 2024. Hydrographic vs. dynamic description of a basin: the example of baroclinic motion in the Ionian Sea. Oceans 5, 383-397. https://doi.org/10.3390/oceans5020023

Eusebi Borzelli, G. L., Napolitano, E., Iacono, R., Struglia, M. V. 2025. Decadal trends in buoyancy, internal modes and horizontal dynamics in the Northern Ionian Sea. Oceans 6, 69. https://doi.org/10.3390/oceans6040069

Gačić, M., Eusebi Borzelli, G. L., Civitarese, G., Cardin, V., Yari, S. 2010. Can internal processes sustain reversals of the ocean upper circulation? The Ionian Sea example. Geophys. Res. Lett. 37, L09608. https://doi.org/10.1029/2010GL043216

Gačić, M., Schroeder, K., Civitarese, G., Cosoli, S., Vetrano, A., Eusebi Borzelli, G. L. 2013. Salinity in the Sicily Channel corroborates the role of the Adriatic-Ionian Bimodal Oscillating System (BiOS) in shaping the decadal variability of the Mediterranean overturning circulation. Ocean Sci. 9, 83-90. https://doi.org/10.5194/os-9-83-2013

Garrabou, J., Gómez-Gras, D., Medrano, A., Cerrano, C., Ponti, M., Schlegel, R., Bensoussan, N., Turicchia, E., Sini, M., Gerovasileiou, V., Teixido, N., Mirasole, A., Tamburello, L., Cebrian, E., Rilov, G., Ledoux, J.-B., Souissi, J. B., Khamassi, F., Ghanem, R., Benabdi, M., Grimes,

S., Ocaña, O., Bazairi, H., Hereu, B., Linares, C., Kersting, D. K., Rovira, G., Ortega, J., Casals, D., Pagès-Escolà, M., Margarit, N., Capdevila, P., Verdura, J., Ramos, A., Izquierdo, A., Barbera, C., Rubio-Portillo, E., Anton, I., López-Sendino, P., Díaz, D., Vázquez-Luis, M., Duarte, C., Marbà, N., Aspillaga, E., Espinosa, F., Grech, D., Guala, I., Azzurro, E., Farina, S., Gambi, M. C., Chimienti, G., Montefalcone, M., Azzola, A., Mantas, T. P., Fraschetti, S., Ceccherelli, G., Kipson, S., Bakran-Petricioli, T., Petricioli, D., Jimenez, C., Katsanevakis, S., Kizilkaya, I. T., Kizilkaya, Z., Sartoretto, S., Rouanet, E., Ruitton, S., Comeau, S., Gattuso, J.-P., Harmelin, J.-G. 2022. Marine heatwaves drive recurrent mass mortalities in the Mediterranean Sea. Glob. Change Biol. 28, 5708-5725. https://doi.org/10.1111/gcb.16301

Guinaldo, T., Voldoire, A., Waldman, R., Saux Picart, S., Roquet, H. 2023. Response of the sea surface temperature to heatwaves during the France 2022 meteorological summer. Ocean Sci. 19, 629-647. https://doi.org/10.5194/os-19-629-2023

Hamdeno, M., Alvera-Azcárate, A. 2023. Marine heatwaves characteristics in the Mediterranean Sea: Case study the 2019 heatwave events. Front. Mar. Sci. 10, 1093760. https://doi.org/10.3389/fmars.2023.1093760

Hersbach, H., Bell, B., Berrisford, P., Hirahara, S., Horányi, A., Muñoz-Sabater, J., Nicolas, J., Peubey, C., Radu, R., Schepers, D., Simmons, A., Soci, C., Abdalla, S., Abellan, X., Balsamo, G., Bechtold, P., Biavati, G., Bidlot, J., Bonavita, M., De Chiara, G., Dahlgren, P., Dee, D., Diamantakis, M., Dragani, R., Flemming, J., Forbes, R., Fuentes, M., Geer, A., Haimberger, L., Healy, S., Hogan, R. J., Hólm, E., Janisková, M., Keeley, S., Laloyaux, P., Lopez, P., Lupu, C., Radnoti, G., de Rosnay, P., Rozum, I., Vamborg, F., Villaume, S., Thépaut, J. 2020. The ERA5 global reanalysis. Q. J. R. Meteorol. Soc. 146, 1999-2049. https://doi.org/10.1002/qj.3803

Hobday, A. J., Alexander, L. V., Perkins, S. E., Smale, D. A., Straub, S. C., Oliver, E. C., Benthuysen, J. A., Burrows, M. T., Donat, M. G., Feng, M., Holbrook, N. J., Moore, P. J., Scannell, H. A., Sen Gupta, A., Wernberg, T. 2016. A hierarchical approach to defining marine heatwaves. Prog. Oceanogr. 141, 227-238. https://doi.org/10.1016/j.pocean.2015.12.014

Hogg, N. G., Stommel, H. M. 1985. Hetonic explosions: The breakup and spread of warm pools as explained by baroclinic point vortices. J. Atmos. Sci. 42, 1465-1476. https://doi.org/10.1175/1520-0469(1985)042<1465:HETBAS>2.0.CO;2

Holbrook, N. J., Gupta, A. S., Oliver, E. C., Hobday, A. J., Benthuysen, J. A., Scannell, H. A., Smale, D. A., Wernberg, T. 2020. Keeping pace with marine heatwaves. Nat. Rev. Earth Environ. 1, 482-493. https://doi.org/10.1038/s43017-020-0068-4

Hoskins, B. J., McIntyre, M. E., Robertson, A. W. 1985. On the use and significance of isentropic potential vorticity maps. Q. J. R. Meteorol. Soc. 111, 877-946. https://doi.org/10.1002/qj.49711147002

Houpert, L., Testor, P., de Madron, X. D., Somot, S., d'Ortenzio, F., Estournel, C., Lavigne, H. 2015. Seasonal cycle of the mixed layer, the seasonal thermocline and the upper-ocean heat storage rate in the Mediterranean Sea derived from observations. Prog. Oceanogr. 132, 333-352. https://doi.org/10.1016/j.pocean.2014.11.004

Ibrahim, O., Mohamed, B., Nagy, H. 2021. Spatial variability and trends of marine heat waves in the Eastern Mediterranean Sea over 39 years. J. Mar. Sci. Eng. 9, 643. https://doi.org/10.3390/jmse9060643

IPCC. 2021. Summary for policymakers, in: Masson-Delmotte, V., Zhai, P., Pirani, A., Connors, S. L., Péan, C., Berger, S., Caud, N., Chen, Y., Goldfarb, L., Gomis, M. I., Huang, M., Leitzell, K., Lonnoy, E., Matthews, J. B. R., Maycock, T. K., Waterfield, T., Yelekçi, O., Yu, R., Zhou, B. 2023. Climate Change 2021: The Physical Science Basis. Contribution of Working Group I to the Sixth Assessment Report of the Intergovernmental Panel on Climate Change.

Cambridge University Press, Cambridge, United Kingdom and New York, NY, USA, 3-32. https://doi.org/10.1017/9781009157896.001

Jebri, F., Zakardjian, B., Birol, F., Bouffard, J., Jullion, L., Sammari, C. 2017. Interannual variations of surface currents and transports in the Sicily Channel derived from coastal altimetry. J. Geophys. Res. Oceans 122, 8330-8353. https://doi.org/10.1002/2017JC012836

Jordà, G., Schuckmann, K. V., Josey, S. A., Caniaux, G., García-Lafuente, J., Sammartino, S., Özsoy, E., Polcher, J., Notarstefano, G., Poulain, P.-M., Adloff, F., Salat, J., Naranjo, C., Schroeder, K., Chiggiato, J., Sannino, G., Macías, D. 2017. The Mediterranean Sea heat and mass budgets: Estimates, uncertainties and perspectives. Prog. Oceanogr. 156, 174-208. https://doi.org/10.1016/j.pocean.2017.07.001

Josey, S. A., Schroeder, K. 2023. Declining winter heat loss threatens continuing ocean convection at a Mediterranean dense water formation site. Environ. Res. Lett. 18, 024005. https://doi.org/10.1088/1748-9326/aca9e4

Jouini, M., Béranger, K., Arsouze, T., Beuvier, J., Thiria, S., Crépon, M., Taupier-Letage, I. 2016. The Sicily Channel surface circulation revisited using a neural clustering analysis of a high-resolution simulation. J. Geophys. Res. Oceans 121, 4545-4567. https://doi.org/10.1002/2015JC011472

Juza, M., Tintoré, J. 2021. Multivariate sub-regional ocean indicators in the Mediterranean sea: from event detection to climate change estimations. Front. Mar. Sci. 8, 610589. https://doi.org/10.3389/fmars.2021.610589

Juza, M., Fernández-Mora, À., Tintoré, J. 2022. Sub-regional marine heat waves in the Mediterranean sea from observations: long-term surface changes, sub-surface and coastal responses. Front. Mar. Sci. 9, 785771. https://doi.org/10.3389/fmars.2022.785771

Kalimeris, A., Kassis, D. 2020. Sea surface circulation variability in the Ionian-Adriatic Seas. Prog. Oceanogr. 189, 102454. https://doi.org/10.1016/j.pocean.2020.102454

Krestenitis, M., Androulidakis, Y., Krestenitis, Y. 2024. Deep learning-based forecasting of sea surface temperature in the interim future: application over the Aegean, Ionian, and Cretan Seas (NE Mediterranean Sea). Ocean Dyn. 74, 149-168. https://doi.org/10.1007/s10236-023-01595-3

Kubin, E., Menna, M., Mauri, E., Notarstefano, G., Mieruch, S., Poulain, P.-M. 2023. Heat content and temperature trends in the Mediterranean Sea as derived from Argo float data. Front. Mar. Sci. 10, 1271638. https://doi.org/10.3389/fmars.2023.1271638

Lascaratos, A., Williams, R. G., Tragou, E. 1993. A mixed-layer study of the formation of Levantine intermediate water. J. Geophys. Res. 98, 14739-14749. https://doi.org/10.1029/93JC00912

Lavigne, H., Civitarese, G., Gačić, M., d'Ortenzio, F. 2018. Impact of decadal reversals of the north Ionian circulation on phytoplankton phenology. Biogeosciences 15, 4431-4445. https://doi.org/10.5194/bg-15-4431-2018

Lima, F. P., Wethey, D. S. 2012. Three decades of high-resolution coastal sea surface temperatures reveal more than warming. Nat. Commun. 3, 704. https://doi.org/10.1038/ncomms1713

Litsi-Mizan, V., Efthymiadis, P. T., Gerakaris, V., Serrano, O., Tsapakis, M., Apostolaki, E. T. 2023. Decline of seagrass (Posidonia oceanica) production over two decades in the face of warming of the Eastern Mediterranean Sea. New Phytol. 239, 2126-2137. https://doi.org/10.1111/nph.19084

Liu, F., Mikolajewicz, U., Six, K. D. 2022. Drivers of the decadal variability of the North Ionian Gyre upper layer circulation during 1910-2010: a regional modelling study. Clim. Dyn. 58, 2065-2077. https://doi.org/10.1007/s00382-021-05714-y

Malanotte-Rizzoli, P., Manca, B. B., Ribera d'Alcalà, M., Theocharis, A., Bergamasco, A., Bregant, D., Budillon, G., Civitarese, G., Georgopoulos, D., Michelato, A., Sansone, E., Scarazzato, P.,

Souvermezoglou, E. 1997. A synthesis of the Ionian Sea hydrography, circulation and water mass pathways during POEM-Phase I. Prog. Oceanogr. 39, 153-204. https://doi.org/10.1016/S0079-6611(97)00013-X

Margirier, F., Testor, P., Heslop, E., Mallil, K., Bosse, A., Houpert, L., Mortier, L., Bouin, M.-N., Coppola, L., d'Ortenzio, F., Durrieu de Madron, X., Mourre, B., Prieur, L., Raimbault, P., Taillandier, V. 2020. Abrupt warming and salinification of intermediate waters interplays with decline of deep convection in the Northwestern Mediterranean Sea. Sci. Rep. 10, 20923. https://doi.org/10.1038/s41598-020-77859-5

Martellucci, R., Paladini de Mendoza, F., Menna, M., Pirro, A., Reale, M., Gačić, M., Poulain, P.-M., Riminucci, F., Le Meur, J., Giordano, P., Langone, L., Cardin, V., Cantoni, C., Bergami, C., Grilli, F., Marini, M., Gallo, A., Notarstefano, G., Toller, S., Bastianini, M., Kralj, M., Diociaiuti, T., Pacciaroni, M., Bussani, A., Miserocchi, S. 2025. A multiobservation analysis of the 2017 dense water formation events: Climate change, bottom density currents, and Adriatic-Ionian sea circulation (Mediterranean Sea). J. Geophys. Res. Oceans 130, e2024JC022306. https://doi.org/10.1029/2024JC022306

Martínez, J., García-Ladona, E., Ballabrera-Poy, J., Isern-Fontanet, J., González-Motos, S., Allegue, J. M., González-Haro, C. 2024. Atlas of surface currents in the Mediterranean and Canary-Iberian-Biscay waters. J. Oper. Oceanogr. 17, 40-62. https://doi.org/10.1080/1755876X.2022.2102357

Marullo, S., Serva, F., Iacono, R., Napolitano, E., Di Sarra, A., Meloni, D., Monteleone, F., Sferlazzo, D., De Silvestri, L., De Toma, V., Pisano, A., Bellacicco, M., Landolfi, A., Organelli, E., Yang, C., Santoleri, R. 2023. Record-breaking persistence of the 2022/23 marine heatwave in the Mediterranean Sea. Environ. Res. Lett. 18, 114041. https://doi.org/10.1088/1748-9326/ad02ae

Meli, M. 2024. The potential recording of North Ionian Gyre's reversals as a decadal signal in sea level during the instrumental period. Sci. Rep. 14, 4907. https://doi.org/10.1038/s41598-024-55579-4

Menna, M., Poulain, P.-M. 2010. Mediterranean intermediate circulation estimated from Argo data in 2003-2010. Ocean Sci. 6, 331-343. https://doi.org/10.5194/os-6-331-2010

Menna, M., Suarez, N. R., Civitarese, G., Gačić, M., Rubino, A., Poulain, P.-M. 2019. Decadal variations of circulation in the Central Mediterranean and its interactions with mesoscale gyres. Deep Sea Res. Part II 164, 14-24. https://doi.org/10.1016/j.dsr2.2019.02.004

Menna, M., Gerin, R., Notarstefano, G., Mauri, E., Bussani, A., Pacciaroni, M., Poulain, P.-M. 2021. On the circulation and thermohaline properties of the Eastern Mediterranean Sea. Front. Mar. Sci. 8, 671469. https://doi.org/10.3389/fmars.2021.671469

Menna, M., Gačić, M., Notarstefano, G., Fedele, G., Mauri, E., Gerin, R., Poulain, P.-M. 2022. Climatic, decadal, and interannual variability in the upper layer of the Mediterranean Sea using remotely sensed and in-situ data. Remote Sens. 14, 1322. https://doi.org/10.3390/rs14061322

Menna, M., Gačić, M., Pirro, A., Mauri, E., Savonitto, G., Pacciaroni, M., Cardin, V., Notarstefano, G., Gallo, A., Zuppelli, P., Bussani, A., Martellucci, R. 2026. Salinity-driven dynamics in the central Mediterranean in the era of ocean warming. Environ. Res. Commun. 8, 045002. https://doi.org/10.1088/2515-7620/ae558a

Mercator Ocean International, 2025. Assessing the Ocean in 2024. France. https://www.mercator-ocean.eu/ocean-news/assessing-the-ocean-in-2024/ (accessed August 2026)

Millot, C., Taupier-Letage, I. 2005. Circulation in the Mediterranean Sea, in: The Mediterranean Sea. Handb. Environ. Chem. 5K, Springer, 29-66. https://doi.org/10.1007/b107143

Mkhinini, N., Coimbra, A. L. S., Stegner, A., Arsouze, T., Taupier-Letage, I., Béranger, K. 2014. Long-lived mesoscale eddies in the eastern Mediterranean Sea: Analysis of 20 years of

AVISO geostrophic velocities. J. Geophys. Res. Oceans 119, 8603-8626. https://doi.org/10.1002/2014JC010176

Mohamed, B., Mohamed, A., Alam El-Din, K., Nagy, H., Shaltout, M. 2019. Inter-annual variability and trends of Sea Level and Sea Surface Temperature in the Mediterranean Sea over the last 25 Years. Pure Appl. Geophys. 176, 3787-3810. https://doi.org/10.1007/s00024-019-02156-w

Napolitano, E., Carillo, A., Struglia, M. V., Iacono, R., Palma, M., Eusebi Borzelli, G. L., Sannino, G. 2025. The role of the Atlantic-Ionian stream in the long-term variability of the surface circulation in the Northern Ionian Sea: Results from a hindcast simulation. Prog. Oceanogr. 234, 103472. https://doi.org/10.1016/j.pocean.2025.103472

Ni, K., Zhai, X., Yang, Z., Chen, D. 2023. Generation of cold anticyclonic eddies and warm cyclonic eddies in the tropical oceans. J. Phys. Oceanogr. 53, 1485-1498. https://doi.org/10.1175/JPO-D-22-0197.1

Ozer, T., Gertman, I., Kress, N., Silverman, J., Herut, B. 2017. Interannual thermohaline (1979-2014) and nutrient (2002-2014) dynamics in the Levantine surface and intermediate water masses, SE Mediterranean Sea. Glob. Planet. Change 151, 60-67. https://doi.org/10.1016/j.gloplacha.2016.04.001

Pastor, F., Valiente, J. A., Palau, J. L. 2018. Sea surface temperature in the Mediterranean: Trends and spatial patterns (1982-2016). Pure Appl. Geophys. 175, 4017-4029. https://doi.org/10.1007/s00024-017-1739-z

Pastor, F., Valiente, J. A., Khodayar, S. 2020. A warming Mediterranean: 38 years of increasing sea surface temperature. Remote Sens. 12, 2687. https://doi.org/10.3390/rs12172687

Pastor, F., Khodayar, S. 2023. Marine heat waves: Characterizing a major climate impact in the Mediterranean. Sci. Total Environ. 861, 160621. https://doi.org/10.1016/j.scitotenv.2022.160621

Patti, B., Torri, M., Placenti, F., Cuttitta, A. 2025. Impact of the Adriatic-Ionian Bimodal Oscillating System (BiOS) on the biodiversity patterns of the larval fish community in the north-eastern sector of the Strait of Sicily (central Mediterranean, Malta Channel). Front. Earth Sci. 13, 1531521. https://doi.org/10.3389/feart.2025.1531521

Pinardi, N., Masetti, E. 2000. Variability of the large scale general circulation of the Mediterranean Sea from observations and modelling: A review. Palaeogeogr. Palaeoclimatol. Palaeoecol. 158, 153-173. https://doi.org/10.1016/S0031-0182(00)00048-1

Pinardi, N., Zavatarelli, M., Adani, M., Coppini, G., Fratianni, C., Oddo, P., Simoncelli, S., Tonani, M., Lyubartsev, V., Dobricic, S., Bonaduce, A. 2015. Mediterranean Sea large-scale low-frequency ocean variability and water mass formation rates from 1987 to 2007: A retrospective analysis. Prog. Oceanogr. 132, 318-332. https://doi.org/10.1016/j.pocean.2013.11.003

Pirro, A., Martellucci, R., Gallo, A., Kubin, E., Mauri, E., Juza, M., Notarstefano, G., Pacciaroni, M., Bussani, A., Menna, M. 2024. Subsurface warming derived from Argo floats during the 2022 Mediterranean marine heat wave. State Planet 4-osr8, 1-12. https://doi.org/10.5194/sp-4-osr8-18-2024

Pirro, A., Martellucci, R., Gallo, A., Mauri, E., Notarstefano, G., Pacciaroni, M., Bussani, A., Menna, M. 2025. Tracking subsurface warming from the 2022 Mediterranean Marine Heatwave using Argo Floats: impacts observed through 2024. Conference presentation, 8th Euro-Argo Science Meeting, Crete, Greece.

Pisano, A., Marullo, S., Artale, V., Falcini, F., Yang, C., Leonelli, F. E., Santoleri, R., Buongiorno Nardelli, B. 2020. New evidence of Mediterranean climate change and variability from sea surface temperature observations. Remote Sens. 12, 132. https://doi.org/10.3390/rs12010132

Poulain, P.-M., Menna, M., Mauri, E. 2012. Surface geostrophic circulation of the Mediterranean Sea derived from drifter and satellite altimeter data. J. Phys. Oceanogr. 42, 973-990. https://doi.org/10.1175/JPO-D-11-0159.1

Reale, M., Cossarini, G., Lazzari, P., Lovato, T., Bolzon, G., Masina, S., Solidoro, C., Salon, S. 2022. Acidification, deoxygenation, and nutrient and biomass declines in a warming Mediterranean Sea. Biogeosciences 19, 4035-4065. https://doi.org/10.5194/bg-19-4035-2022

Schaeffer, A., Roughan, M. 2017. Subsurface intensification of marine heatwaves off southeastern Australia: The role of stratification and local winds. Geophys. Res. Lett. 44, 5025-5033. https://doi.org/10.1002/2017GL073714

Simon, A., Pires, C., Frölicher, T. L., Russo, A. 2023. Long-term warming and interannual variability contributions to marine heatwaves in the Mediterranean. Weather Clim. Extremes 42, 100619. https://doi.org/10.1016/j.wace.2023.100619

Simoncelli, S., Oliveri, P., Mattia, G., Myroshnychenko, V., Barth, A., Troupin, C. 2020a. SeaDataCloud Temperature and Salinity Climatology for the Mediterranean Sea (Version 2). Product Information Document (PIDoc). SeaDataCloud. https://doi.org/10.13155/77514

Simoncelli, S. 2020b. SeaDataCloud Mediterranean Sea - V2 Temperature and Salinity Climatology. Ifremer [data set]. https://doi.org/10.12770/3f8eaace-9f9b-4b1b-a7a4-9c55270e205a

Sivakumar, A., Weiss, J. B. 2022. Volume transport by a 3D quasigeostrophic heton. Fluids 7, 92. https://doi.org/10.3390/fluids7030092

Skliris, N., Zika, J. D., Herold, L., Josey, S. A., Marsh, R. 2018. Mediterranean sea water budget long-term trend inferred from salinity observations. Clim. Dyn. 51, 2857-2876. https://doi.org/10.1007/s00382-017-4053-7

Smith, K. E., Burrows, M. T., Hobday, A. J., Sen Gupta, A., Moore, P. J., Thomsen, M., Wernberg, T., Smale, D. A. 2021. Socioeconomic impacts of marine heatwaves: Global issues and opportunities. Science 374, 6566, eabj3593. https://doi.org/10.1126/science.abj3593

Song, X., Yu, L. 2017. Air-sea heat flux climatologies in the Mediterranean Sea: Surface energy balance and its consistency with ocean heat storage. J. Geophys. Res. Oceans 122, 4068-4087. https://doi.org/10.1002/2016JC012254

Soukissian, T., Karathanasi, F., Axaopoulos, P., Voukouvalas, E., Kotroni, V. 2018. Offshore wind climate analysis and variability in the Mediterranean Sea. Int. J. Climatol. 38, 384-402. https://doi.org/10.1002/joc.5182

Terzić, E., Vilibić, I. 2026. Twenty-first century thermohaline trends and abrupt shifts in the Ionian Sea. Front. Mar. Sci. 12, 1718186. https://doi.org/10.3389/fmars.2025.1718186

Trigo, R., Barriopedro, D., Garrido-Pérez, J., Simon, J., Plecha, S., Teles-Machado, A., Russo, A., García-Herrera, R. 2025. The outstanding European and Mediterranean heatwave activity during summer 2022. Atmos. Res. 323, 108195. https://doi.org/10.1016/j.atmosres.2025.108195

Tsimplis, M. N., Zervakis, V., Josey, S. A., Peneva, E. L., Struglia, M. V., Stanev, E. V., Theocharis, A., Lionello, P., Malanotte-Rizzoli, P., Artale, V., Tragou, E., Oguz, T. 2006. Changes in the oceanography of the Mediterranean Sea and their link to climate variability, in: Mediterranean Climate Variability. Dev. Earth Environ. Sci. 4, 227-282. https://doi.org/10.1016/S1571-9197(06)80007-8

United Nations Environment Programme, 2021. Biological diversity in the Mediterranean. Greece. https://www.unep.org/unepmap/resources/factsheets/biological-diversity (accessed August 2026)

Wehde, H., Schuckmann, K. V., Pouliquen, S., Grouazel, A., Bartolome, T., Tintore, J., De Alfonso Alonso-Munoyerro, M., Carval, T., Racapé, V., ISTAC team. 2025. Quality Information

Document. In Situ Thematic Assembly Centre. E.U. Copernicus Marine Service Information (CMEMS).

# Contributions

Table specifying which parts of the thesis are the result of the student's own work and which parts were provided by other team members or collaborators.

| Category | Contributor(s) |
|---|---|
| Writing | Zoé Genet |
| Production of results (except for the following figures) | Z. Genet |
| Figure 6 | Annunziata Pirro and Milena Menna |
| Figure 7 | Riccardo Martellucci and A. Pirro |
| Figure S9 | M. Menna |
| Interpretation of results and discussion | Z. Genet (with discussions with A. Pirro, Aida Alvera-Azcárate and M. Menna) |
| Thesis Review and revision | A. Pirro, A. Alvera-Azcárate, M. Menna |

# Appendix

Supplementary figures: Figures S1-S9

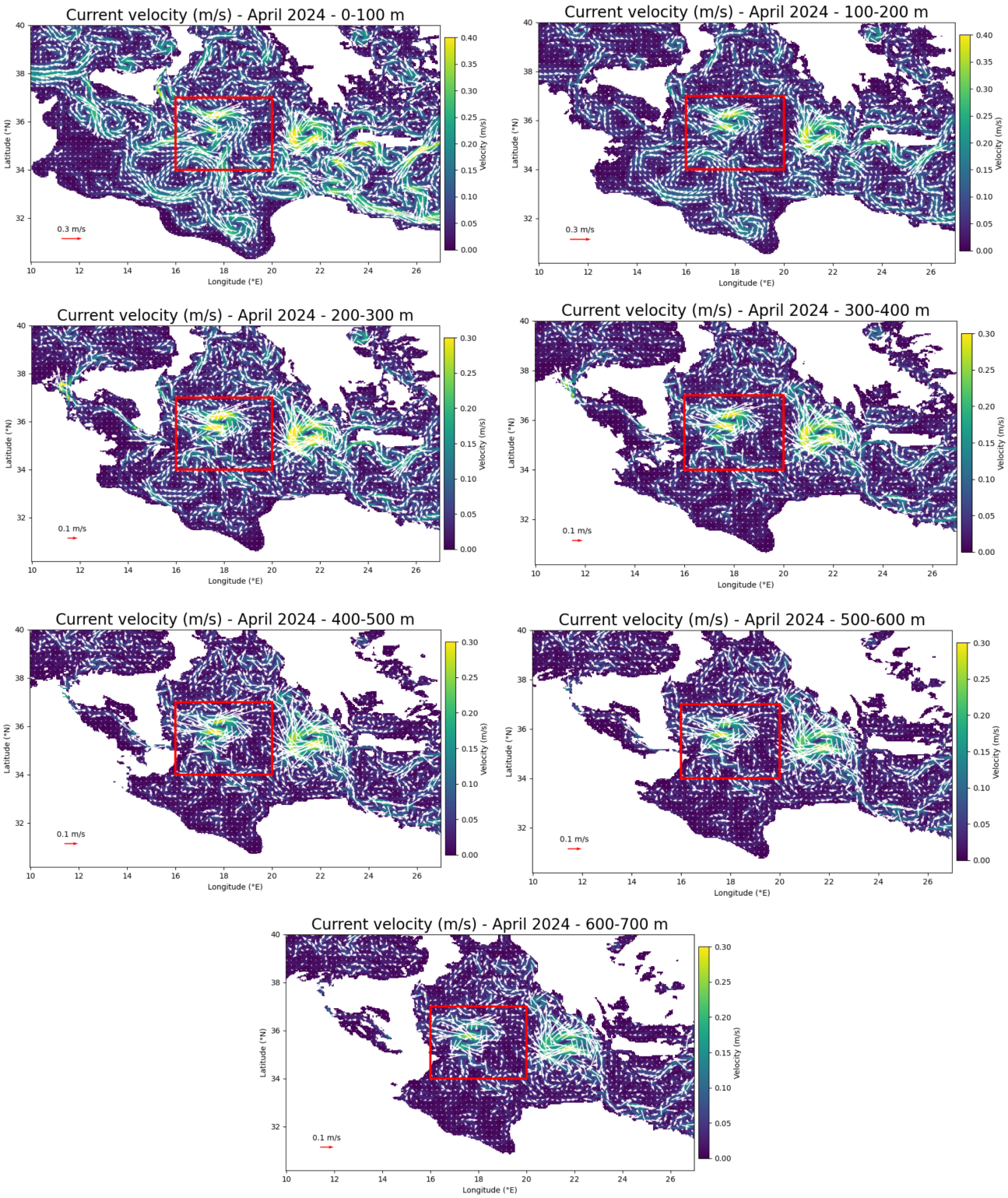


Figure S1: Current velocities from 0 m to 700m deep over the Ionian Sea in April 2024. The study area's borders are highlighted in red.

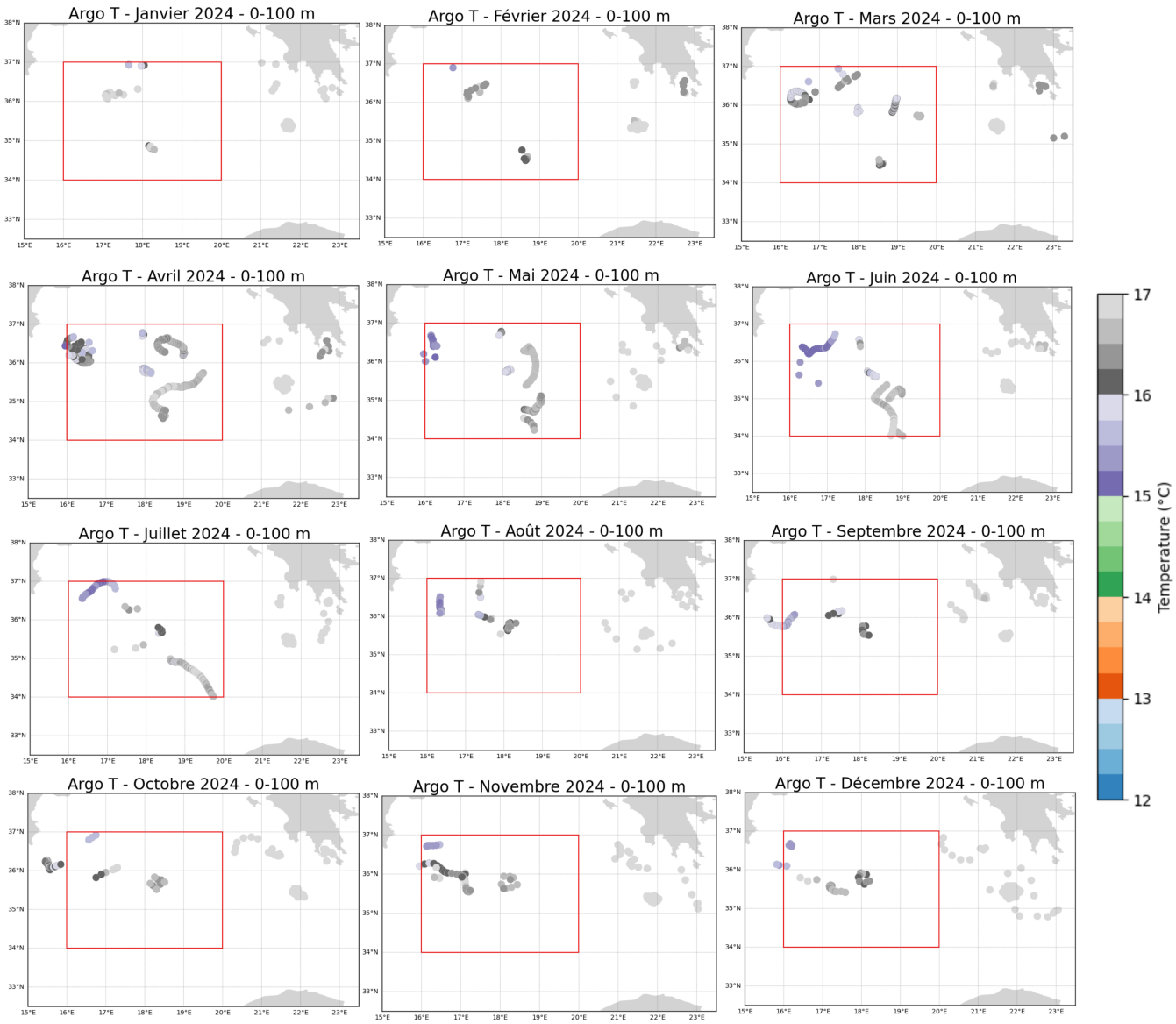


Figure S2: Temperatures measured by Argo floats between 0-100 m in 2024 in the Ionian Sea. The study area's borders are highlighted in red.

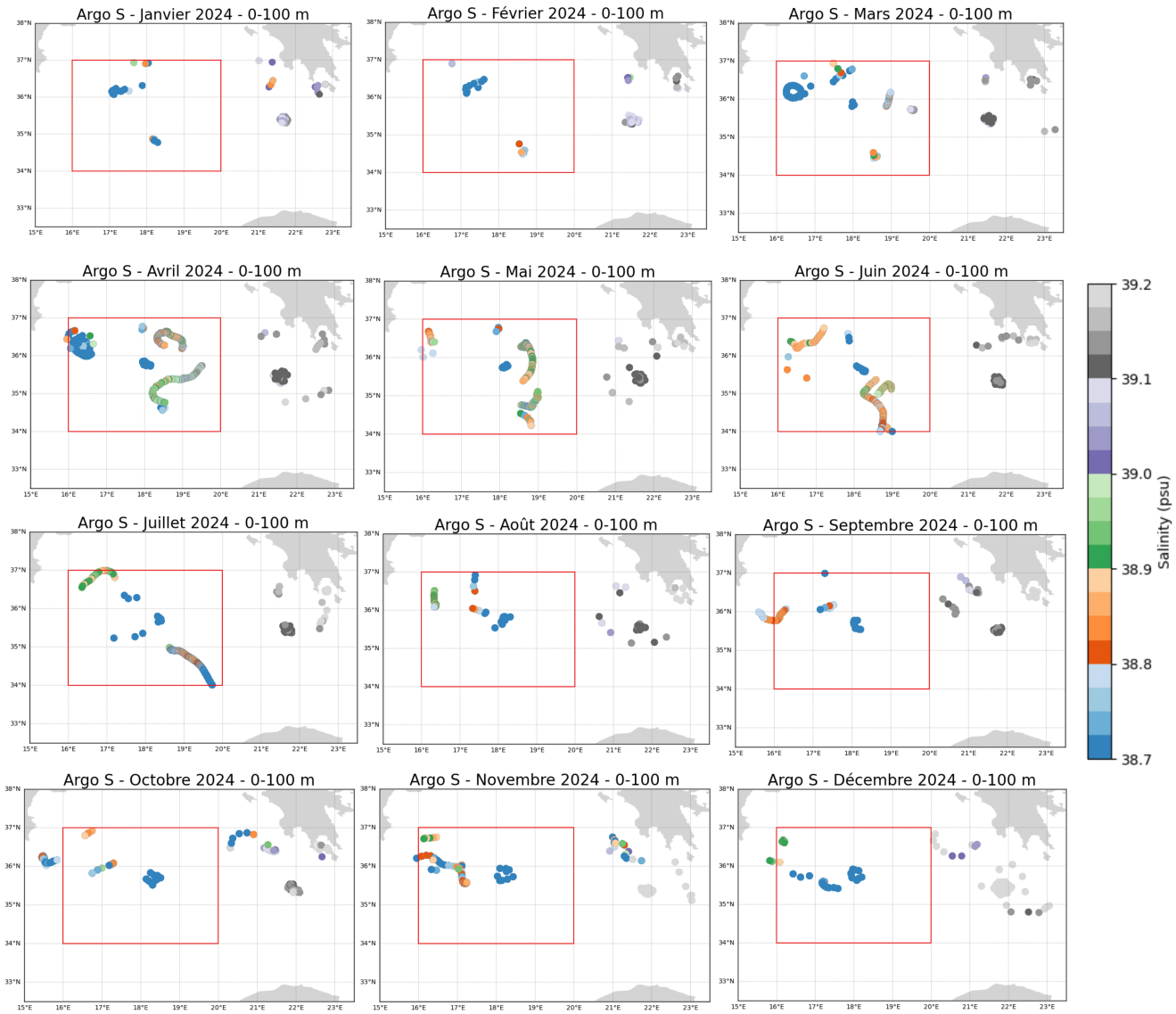


Figure S3: Salinities measured by Argo floats between 0-100 m in 2024 in the Ionian Sea. The study area's borders are highlighted in red.

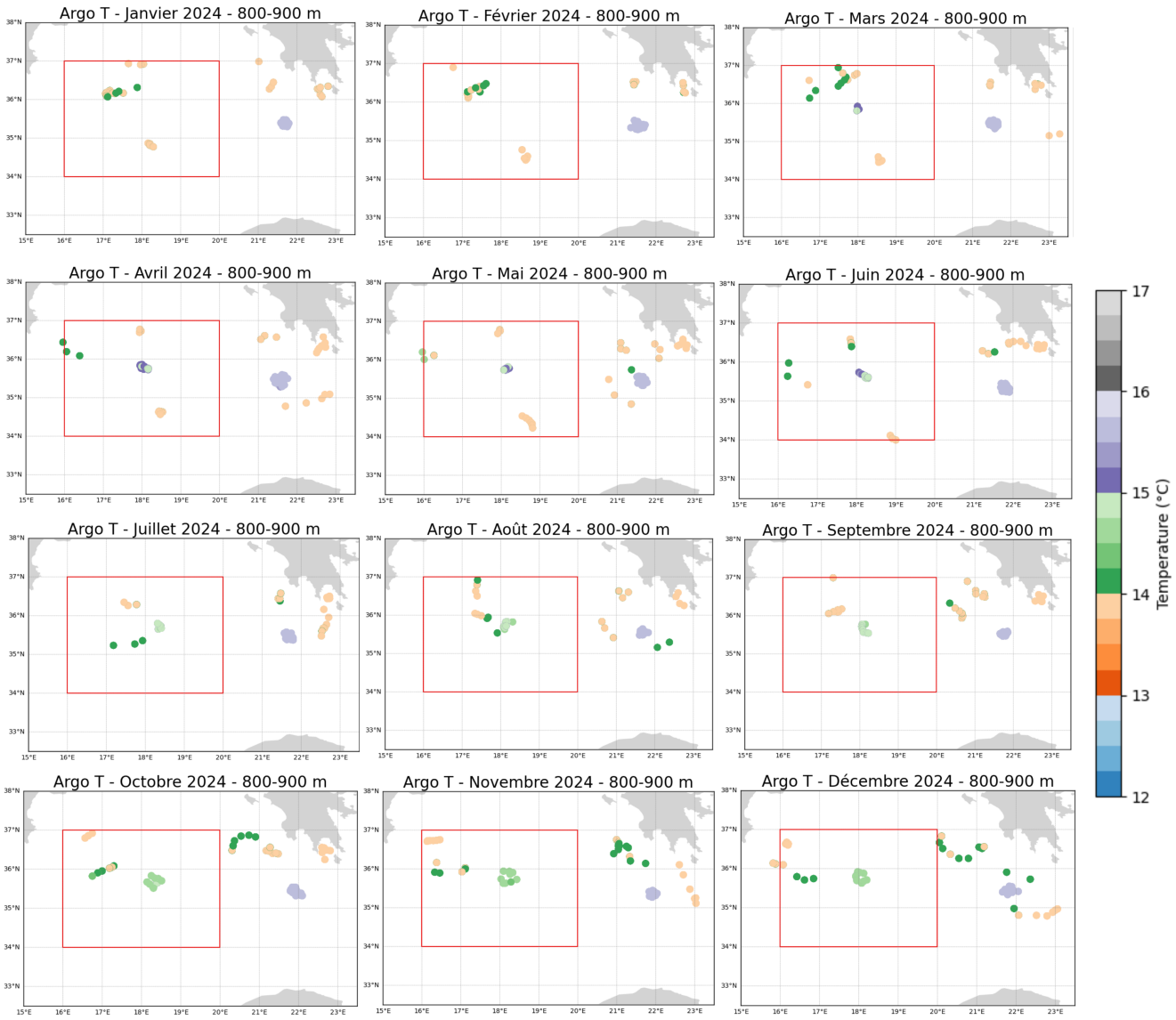


Figure S4: Temperatures measured by Argo floats between 800-900 m in 2024 in the Ionian Sea. The study area's borders are highlighted in red.

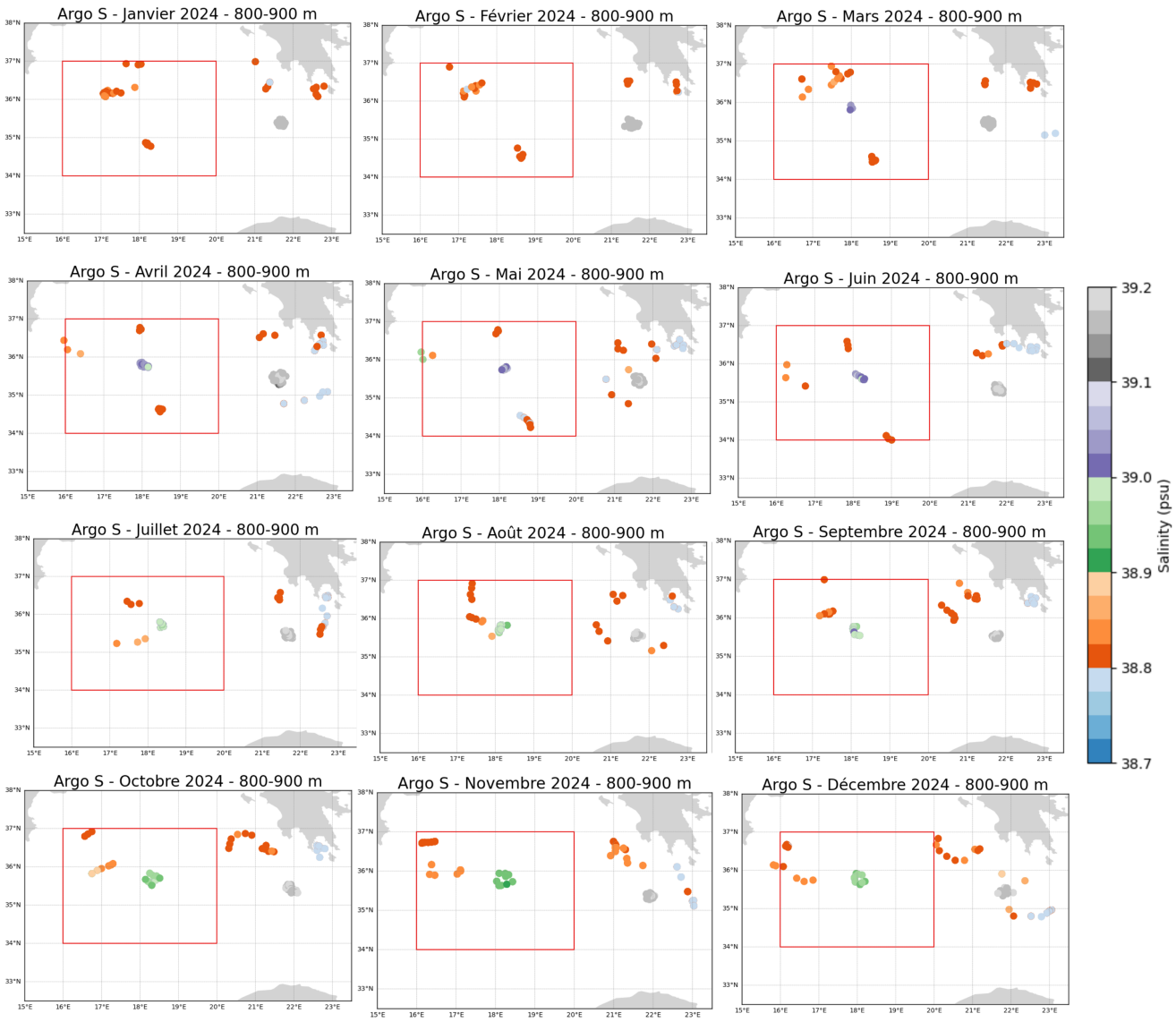


Figure S5: Salinities measured by Argo floats between 800-900 m in 2024 in the Ionian Sea. The study area's borders are highlighted in red.

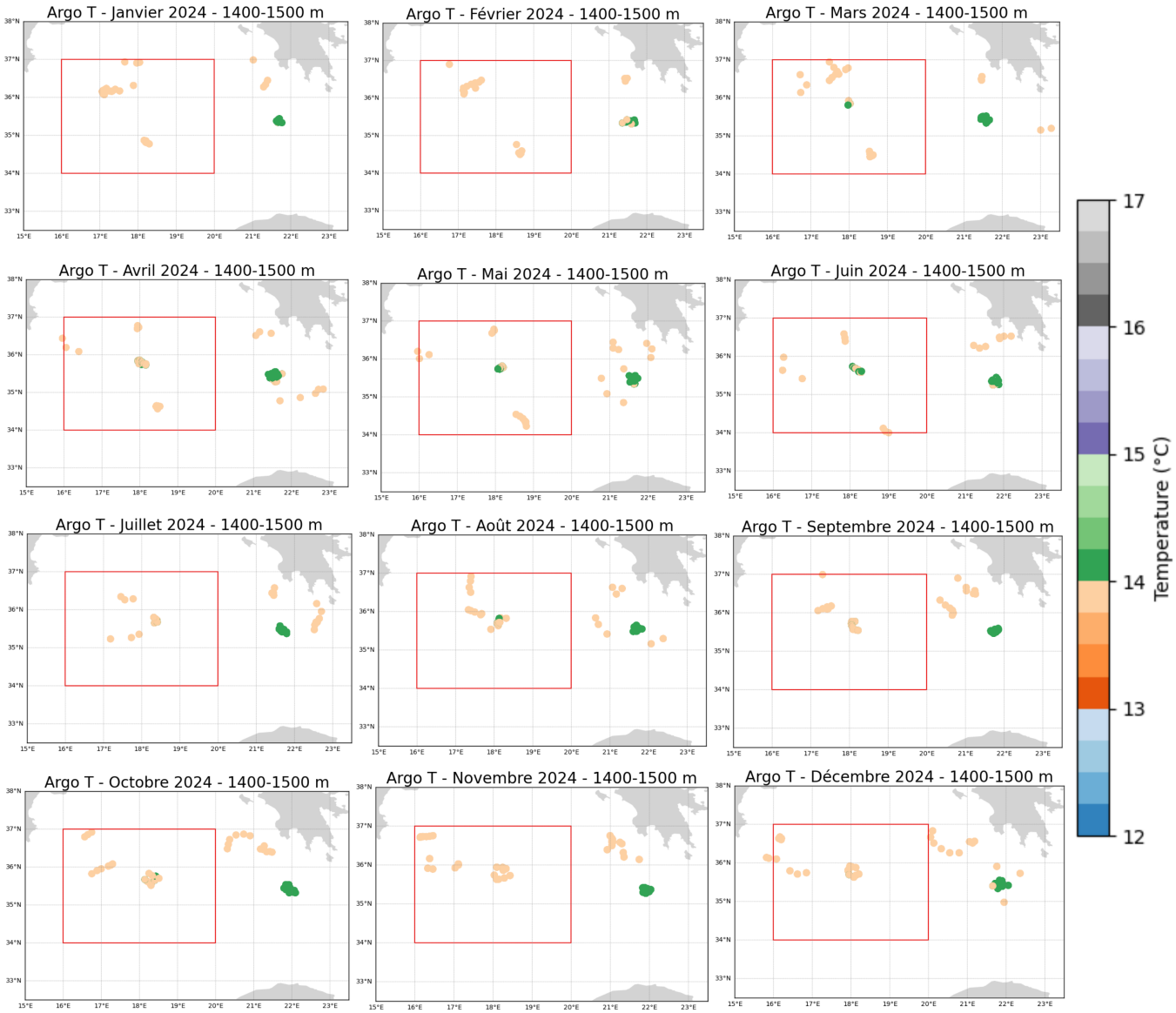


Figure S6: Temperatures measured by Argo floats between 1400-1500 m in 2024 in the Ionian Sea. The study area's borders are highlighted in red.

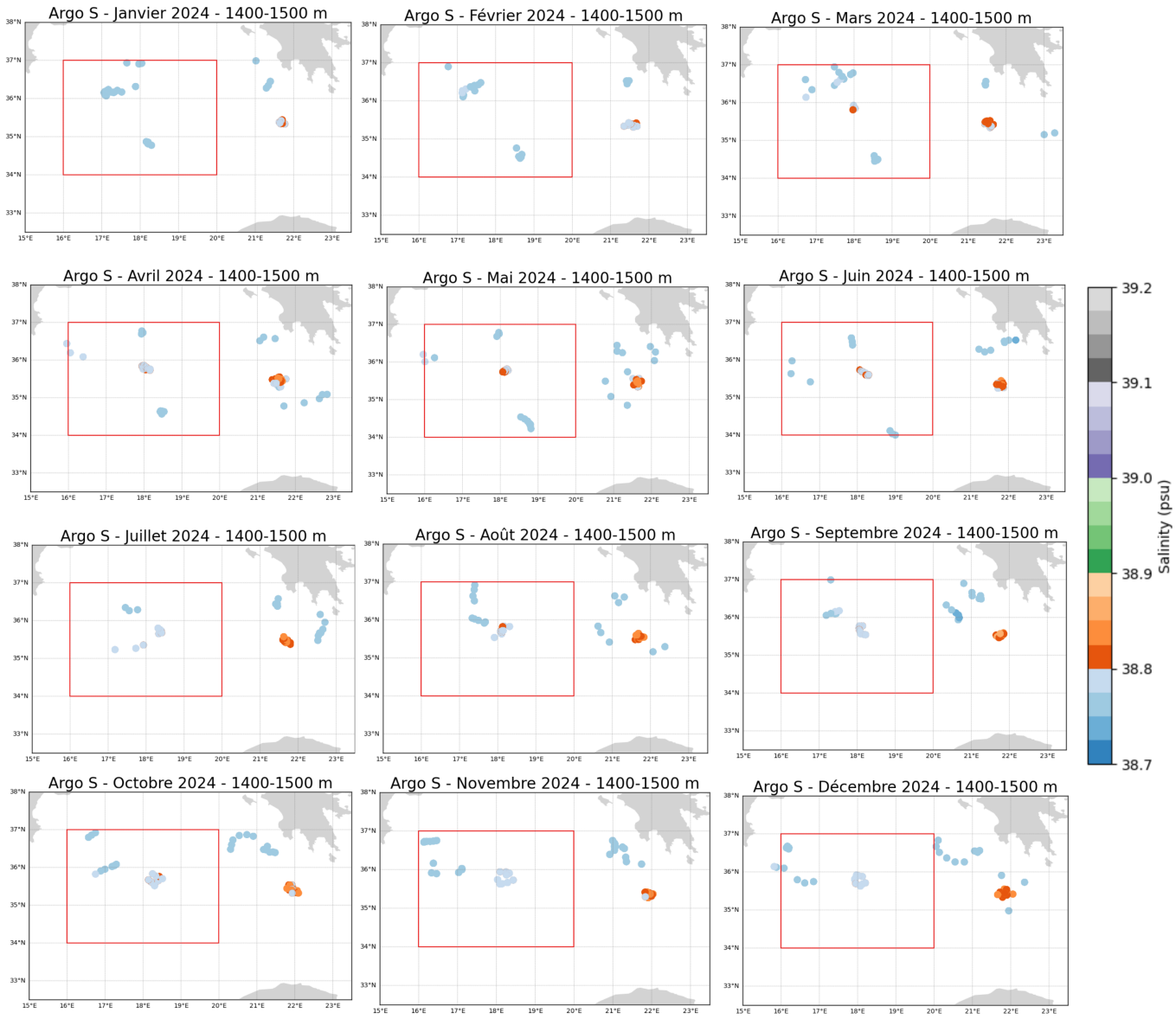


Figure S7: Salinities measured by Argo floats between 1400-1500 m in 2024 in the Ionian Sea. The study area's borders are highlighted in red.

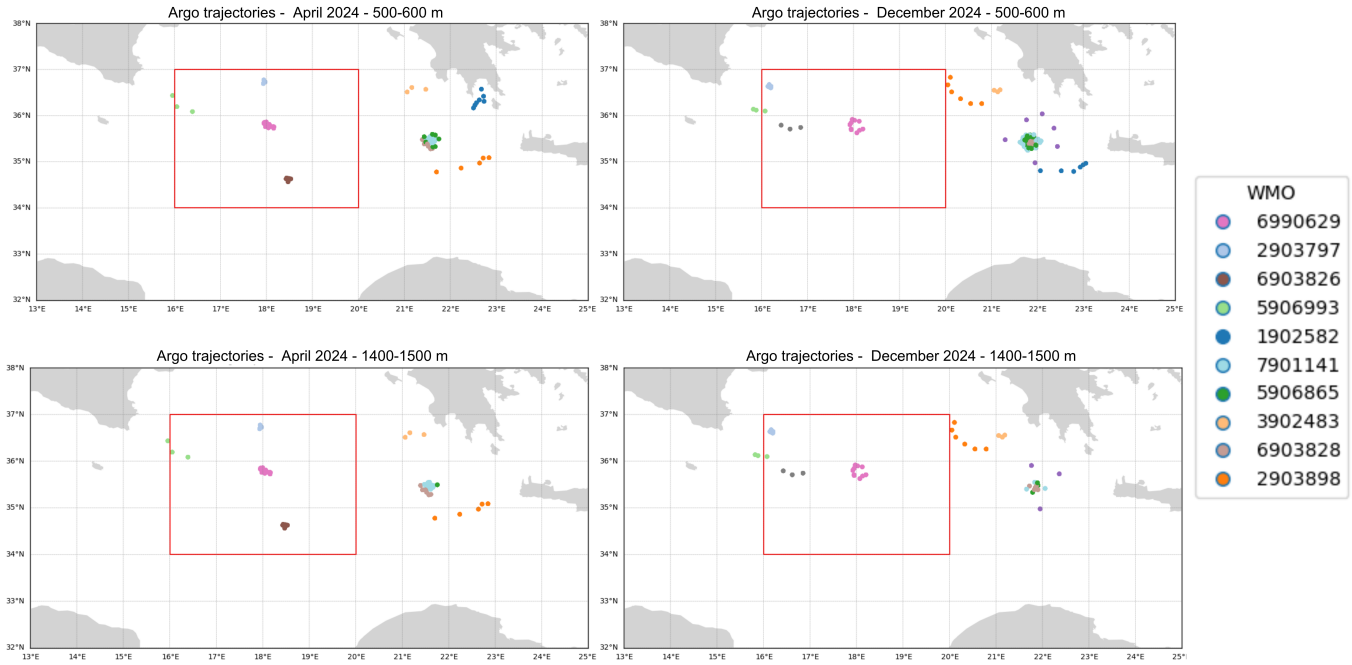


Figure S8: Spatial repartition of Argo floats in the Ionian Sea in April 2024 and December 2024 between 500-600 m and 1400-1500 m depth. The study area's borders are highlighted in red.

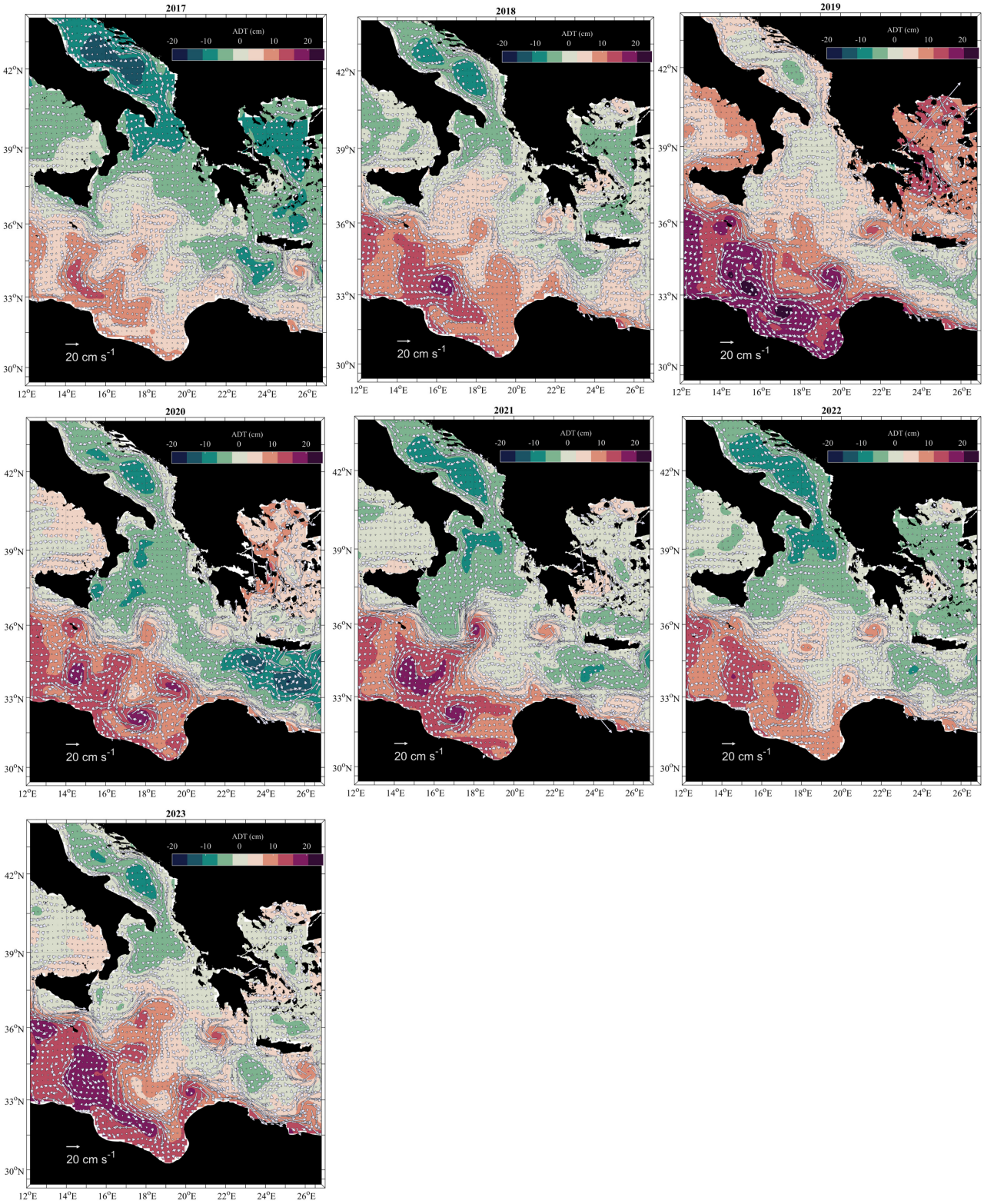


Figure S9: Currents and absolute dynamic topography in the Ionian Sea 2017-2023. An anticyclone is present throughout the years around 36°N and 18°E. Figure by Menna, personnal communication.